An investigation of the internal airflow system behavior of a Turbosail

S.R. Boonstra

TU Delft

An investigation of the internal airflow system behavior of a Turbosail

by

S.R. Boonstra

to obtain the degree of Master of Science
at the Delft University of Technology,
to be defended publicly on Monday March 16, 2020 at 10:00 AM.

Student number:	4141520	
Project duration:	January 1, 2019 – March 16, 2020	
Thesis committee:	Dr. ir. A. Vrijdag,	TU Delft, supervisor
	Ir. K. Visser,	TU Delft
	Dr. ir. P. R. Wellens,	TU Delft

An electronic version of this thesis is available at `http://repository.tudelft.nl/`.

TU Delft

Abstract

The awareness of the climate change is increasing and the effect of air-pollution is irrefutable. To decrease the emissions of large ships the required amount of fuel has to be minimized. This is done by increasing the efficiency of the engine, decreasing the hull resistance or by lowering the cruise speed. Another interesting way of decreasing the emission is by using Wind Assisted Ship Propulsion (WASP). The Turbosail is a promising type of wind propulsion for this purpose introduced by Jacques Cousteau[4]. The Turbosail is an aspirated wing which is able to generate up to 3 times more lift compared to a non aspirated wing. A lot of research has been done in order to increase the performance of the Turbosail. But this research has mainly been done on the outside of the Turbosail and the suction area is often modelled as an area with a uniform flow. In this research a model has been made in order to give insight in the behaviour and sensitivity of the suction system of the Turbosail.

First the model foundation is described. A lumped parameter approach is chosen and the structure of the model is described. The model of the fan is described and after this the total model is made using Matlab Simulink. This model is made such that the number of elements (the amount of parts that the Turbosail is divided in) can be easily varied. This is done in order to perform a convergence study. Followed by a mathematical verification with carefully chosen tests the model is considered as verified.

To understand the sensitivity of different parameters of the system a parameter variation is performed. Different parameters are varied and their effects are simulated. This yields insight in the sensitivity of the system and can be used in order to optimize the energy efficiency of the total suction system.

Finally two possible improved designs are simulated combined with their decrease in power consumption. These results can be used for future simulations and designs with the main purpose to decrease the energy consumption of the shipping industry.

Preface

This thesis report is written by Sjoerd Boonstra as fulfillment of the study Marine Technology, Marine Engineering at the Delft University of Technology. In this thesis report the principles behind the Turbosail, the earlier work and the research done will be discussed.

The personal goal of this research is to erect knowledge in order to improve the energy efficiency and performance of Wind Assisted Ship Propulsion devices. After getting familiar with the Ventifoil, the Turbosail of Econowind, I have noticed that a lot of effort has been spent on the outer geometry. But in each research the suction was assumed to be evenly distributed and in several prototypes this has been done by using relatively small suction holes. To improve future Computational Fluid Dynamics (CFD) calculations and possible prototypes, a model is made to gain insight in the behaviour, performance and the important parameters of the suction system.

I would like to thank Arthur Vrijdag for his great support throughout the project, Bart Koek for his effort in making the basis of the Matlab code and also René Boonstra and Aris de Fijter for their review on the report. Further I would like to thank my friends and colleagues at HedoN Electronic Developments for their support, opportunities, distraction and great humour.

My parents, brother and girlfriend deserve a special note, you motivated me, supported me and comforted me throughout both my Bachelor mechanical engineering and Master maritime engineering. Despite studying is not my favorite activity, I have succeeded in completing this study, something I could not have done without these great people. Personally I like to refer to the following quote accredited to Albert Einstein: *"Everybody is a genius. But if you judge a fish by its ability to climb a tree, it will live its whole life believing that it is stupid."*. For me, this quote depicts the fact that the current educational system does not suits everybody perfect. But sometimes the fish has a tree to climb in order to achieve his goal, something the fish often considers as an impossible task. The fish will think he is stupid, or just not good enough. Other fish around him will give up, while some monkeys will overtake him easily. Stubborn as he is, the fish keep trying, one branch at the time, encouraged by his family and friends. A wind gust throws the fish of the branch, back into the water where he started, but the fish keeps trying. Eventually the fish almost reaches the top of the tree, just one branch to go. That last branch is this thesis, finishing this thesis enables the fish to reach the top of the tree. From this position the fish is able to look around, to other ponds, rivers and even seas. Finally the fish jumps of out the tree, into the water of his choice. Back into the water the fish can finally do what he enjoys and where he is good at, swimming.

Thank you for reading this and I hope you will enjoy reading my thesis.

S.R. Boonstra
Delft, February 2020

Contents

List of Figures

Nomenclature

$\dot{m}$	Mass flow	$\frac{kg}{s}$
η	Kinematic viscosity	$\frac{m^2}{s}$
η_{Fan}	Fan efficiency	–
η_{Motor}	Motor efficiency	–
$\frac{d\omega}{dt}$	Angular acceleration	$\frac{rad}{s^2}$
κ	Permeability factor	–
λ	Darcy friction factor	–
ω	Rotational speed	$\frac{rad}{s}$
π_1	Dimensionless volume flow	–
π_2	Dimensionless pressure	–
ρ	Density	$\frac{kg}{m^3}$
τ	Wall thickness coefficient	–
ζ	Pressure loss coefficient	–
A	Surface area	m^2
A_0	Total area of the perforated sheet	m^2
A_1	Total perforated area of the perforated sheet	m^2
A_p	Projected wing area	m^2
c	Chord length	m
C_a	Aspiration power coefficient	–
C_q	Suction coefficient	–
C_x	Drag coefficient	–
C_z	Lift coefficient	–
c_{avg}	Average chord length	m
D	Diameter	m
F	Force	N
F_x	Drag	N
F_z	Lift	N
I	Current	A
J_{Fan}	Fan moment of inertia	$kg \cdot m^2$
J_{Motor}	Motor moment of inertia	$kg \cdot m^2$

k	Roughness number	–
k_a	Karman's constant	–
L	Length	m
$L_{Element}$	Length of an element	m
$L_{Turbosail}$	Length of the Turbosail	m
m	Mass	kg
$N_{Elements}$	Amount of elements	–
$N_{Holesperelement}$	Amount of holes per element	–
N_{Holes}	Amount of holes	–
p	Pressure	Pa
P_a	Aspiration power	W
p_{in}	Incoming pressure	Pa
p_{loss}	Pressure loss	Pa
p_{out}	Outgoing pressure	Pa
Q	Volumetric flow	$\frac{m^3}{s}$
R	Gas constant	$\frac{J}{kg \cdot K}$
r	Radius	m
Re	Reynolds number	–
Ro	Roughness number	–
T	Temperature	K
t	Time	s
T_{Fan}	Fan torque	Nm
T_{Motor}	Motor torque	Nm
U	Voltage	V
U_w	Wind speed	$\frac{m}{s}$
V	Volume	m^3
v	Velocity	$\frac{m}{s}$
z	Height	m
$w_{perforation}$	Width of the perforated surface	m

1 Introduction

The urgency to reduce the emission of greenhouse and other harmful gasses is rising. To pursue this reduction the International Maritime Organization (IMO) has made regulations. One of the regulations is the reduction of SO_X emission in 2020 to 0.5% mass content in the fuel content[3]. Another method to decrease emissions are Emission Control Areas. These areas are under strict regulations to decrease the amount of harmful emissions like SO_X, NO_X, CO_2 and particle matter. SO_X emissions can be reduced by taking out the sulphur content out of the fuel before the fuel is being burned. NO_X emissions are not a fuel-bound emission. This is because the nitrogen enters the combustion cycle as it is the main component of air. The burned nitrogen is the result of a high combustion temperature that can occur in a diesel engine which causes the nitrogen to react with the present oxygen. To reduce this emission the peak temperature in the cylinders must be lowered, this can be done by reducing the maximum pressure inside the cylinder or by using other geometries to avoid "Hot-spots"[9]. A Hot-spot is an area inside the cylinder where during the combustion the peak temperatures are reached. The emission of particle matter consist out of sooth, due to incomplete combustion, and other particles that are present in the air or fuel. All these emissions are linked to the amount of fuel required to propel the ship. The simplest way reduce all emissions is by reducing the required amount of fuel.

One way to reduce the amount of fuel required to propel the ship is by using a hybrid propulsion system. Wind energy is a well available power source which is already used as a propulsion source. But the strength and direction of the wind is of great importance to make it useful. Combined with the diesel engine this hybrid system will result in a continuously operable but more fuel efficient type of propulsion. This way of propelling a vessel is not new, the Dynarig, the kite and Flettner rotor are already seen in several concepts or have been used in practice (See Figures 1.1, 1.2 and 1.3). Another principle is the Turbosail. This type of wind propulsion is developed by the French oceanographer Jacques-Yves Cousteau and it uses a wing-like sail with a movable flap[4]. This wing has a unconventional high lift-coefficient due to the usage of boundary layer suction. To create this suction along the wing a fan is needed that must be driven by an electric motor. The Turbosail was built and used on a vessel named the Alcyone in 1985, a vessel which still exists. The oil crisis in 1979 induced the search to alternative energy sources. Due to the corresponding high oil prices the economical feasibility of a system as the Turbosail was increased. Nevertheless large scale application did not happen because the oil prices dropped before it was implemented and the interest in renewable energy sources decreased.

Figure 1.1: Dynarig [19]

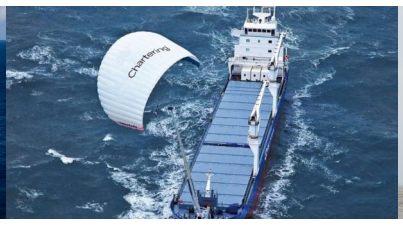

Figure 1.2: Kite [20]

Figure 1.3: Flettner rotor [26]

Nowadays with a higher oil price and the upcoming emission regulations the economic feasibility is reconsidered by the company Econowind and they estimated the Turbosail concept as economically feasible. This resulted in new research and the building of multiple prototypes of their own Turbosail which they call the “Ventifoil”. Their idea is to use a standard 40ft container and to equip it with two Ventifoils each having a length of 11 meters. This container can be positioned on deck of conventional merchant vessels to lower their fuel usage. Anton Kisjes [12] and Laurens-Jan Lagendijk [13] already have done intensive research in the field of wind velocities and pressure distributions by varying the shape, suction strength and position using Computational Fluid Dynamics (CFD).

The aim of this research is to gain knowledge which helps to improve the performance of the Turbosail. The first step will be to gain insight in the working principle and explore previous research. This will lead to the identification of a knowledge gap.

1.1. The operating principle of the Turbosail

The Turbosail is an ovaloid shaped wing which uses boundary layer suction to prevent the boundary layer from separating. In the next subsections different aspects of the Turbosail will be described. First boundary layer separation will be considered, followed by boundary layer suction and the suction system. After that the effect of boundary layer suction on the lift and drag coefficient will be discussed and finally the operating conditions and existing prototypes.

1.1.1. Boundary layer separation

Boundary layer separation is the effect where the flow at the low pressure side of a wing has an adverse pressure gradient which causes the flow to separate from the surface as is shown in Figure 1.4. This effect is better known in aviation as "stall". The separation results in a drop in lift, thus performance. In aviation this drop in lift can be disastrous due to the fact that the aircraft will not be able to fly. In case of hybrid ship propulsion a separating boundary layer will cause the ship to use more fuel due to the fact that a larger part of the propulsive power has to come from the diesel engine. The next subsection will explains how boundary layer can be avoided.

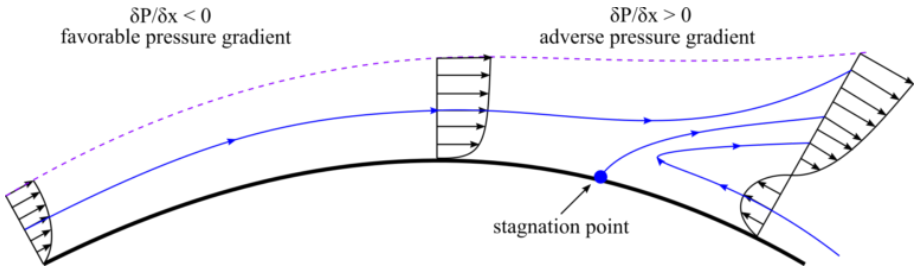

Figure 1.4: Boundary layer separation [2]

1.1.2. Boundary layer suction

One way to overcome boundary layer separation is to suck the boundary layer into the wing. The effect of this boundary layer suction is shown in Figure 1.5. In the left picture boundary layer separation occurs, causing a large wake. In the right picture, the one with boundary layer suction, the separating boundary layer is located further aft. This results in a smaller wake and an increase in lift.

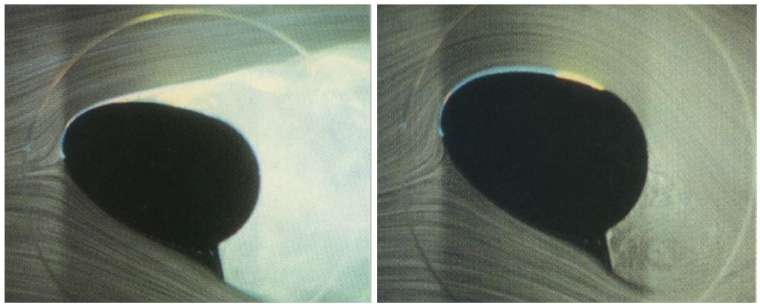

Figure 1.5: Left: airflow without suction, Right: airflow with suction[16]

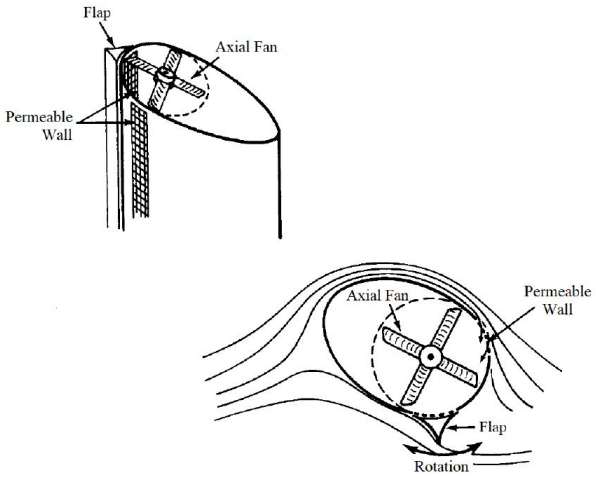

Figure 1.6: Sketch of the Turbosail suction system [16]

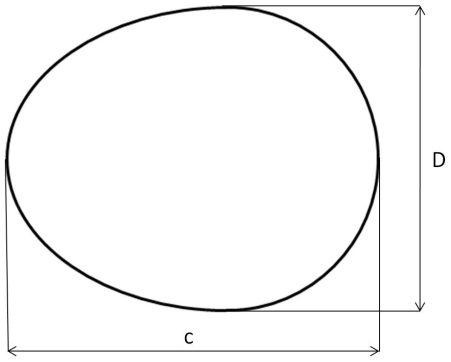

Figure 1.7: The definition of chord and diameter

1.1.3. Suction system

To establish this suction a permeable wall combined with a pressure difference is necessary. This is realised by perforating the Turbosail at the suction location and creating a flow through this perforation using a fan. This fan can be located at the bottom or top of the Turbosail. In Figure 1.6 this setup is depicted. Here the placement of the permeable wall, flap and fan is shown. The flap on the Turbosail can be rotated from one side to the other, in that way the wing is able to "tack" which gives the system the ability to sail in both directions [16]. An interesting engineering feature is that the flap covers the permeable wall at the high pressure side of the wing whereby one moving part, the flap, has a dual function.

1.1.4. The effect of suction on the lift and drag

Boundary layer suction is applied in order to increase the lift. The lift coefficient is defined by Equation 1.1 and the drag coefficient is defined by Equation 1.2. Where U_w is the wind speed and A_p is the projected wing area and Q is the volumetric flow through the suction system. The amount of suction is defined by the suction coefficient C_q (see Eq. 1.3).

$$C_z = \frac{F_z}{\frac{1}{2}\rho A_p U_w^2} \tag{1.1}$$

$$C_x = \frac{F_x}{\frac{1}{2}\rho A_p U_w^2} \tag{1.2}$$

$$C_q = \frac{Q}{A_p U_w} \tag{1.3}$$

Where A_p is defined by the average chord length times the length of the Turbosail:

$$A_p = c_{avg} L_{Turbosail} \tag{1.4}$$

The definition of chord length is shown in Figure 1.7. Also the definition of the diameter D is seen in this figure, this diameter will be used as main parameter in this thesis.

Figure 1.8 shows the trend of lift and drag coefficients for different amounts of suction over a range of angles of attack. Where the amount of suction is quantified by Malavard using C_q. The figure shows that the suction has a large effect on the generated lift: it reaches a lift coefficient of approximately 8.5 at a suction coefficient of 0.047. The increase in drag is relatively small compared to the gain in lift.

1.1.5. Operating conditions

In operation conditions a Turbosail is installed on the deck of a ship. The effect of this ship is not only that it is sailing with a certain speed and direction but the ship also distorts the wind velocity field.

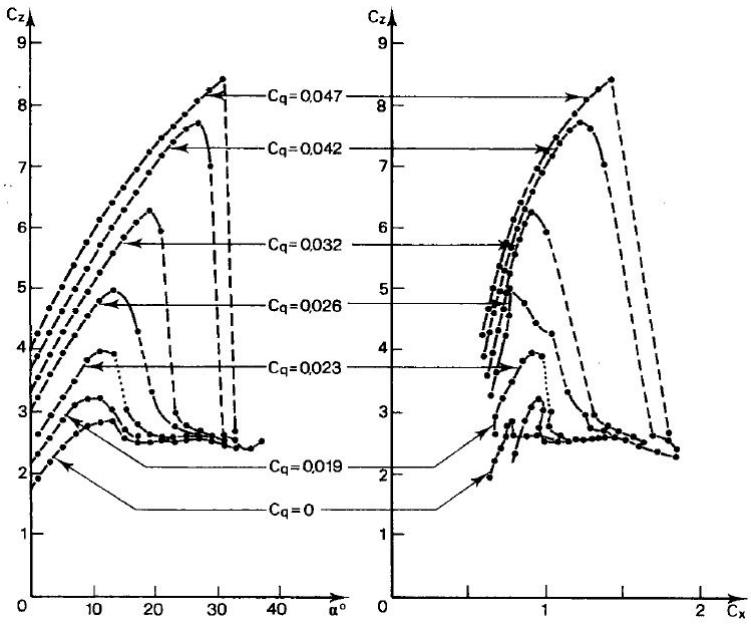

Figure 1.8: Lift and drag coefficients for different C_q and angles of attack [16]

A simple way to describe the wind velocity field at sea is by using a logarithmic speed profile as is showns in Equation 1.5 [25]. Where U is the wind speed in $\frac{m}{s}$, $k_a = 0.4$ is the Karman's constant, z is the height, u^* is the friction velocity and z_0 is the terrain roughness parameter. The roughness parameter is between 0.0001 and 0.01 for open sea with waves. And the friction velocity is set on 0.375 $\frac{m}{s}$. This yields a wind velocity profile as is shown in Figure 1.9. This profile depicts a horizontal velocity field with a velocity of 10.8$\frac{m}{s}$ at 10 meter height and a roughness parameter of 0.0001.

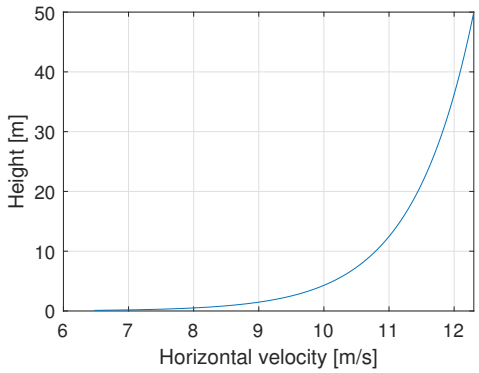

Figure 1.9: The horizontal wind velocity profile at sea

$$U_w(z) = \frac{U_w^*}{k_a} \ln \frac{z}{z_0} \tag{1.5}$$

As stated above, this wind velocity field is affected by the presence of the ship. Moat et al. [17] have modeled this effect and the result can be seen in Figure 1.10. The percentages depict the difference in horizontal flow velocity. Tests of Econowind, which will be discussed in the next subsection, are performed on the 'Lady Christina' of the shipping company 'Wijnne Barends'. Estimated is that the deck is approximately 6 meters above the waterline. The effects of the velocity profile and the flow field distortion diminish one another which results in the assumption for this report to consider the wind across the Turbosail to be uniform.

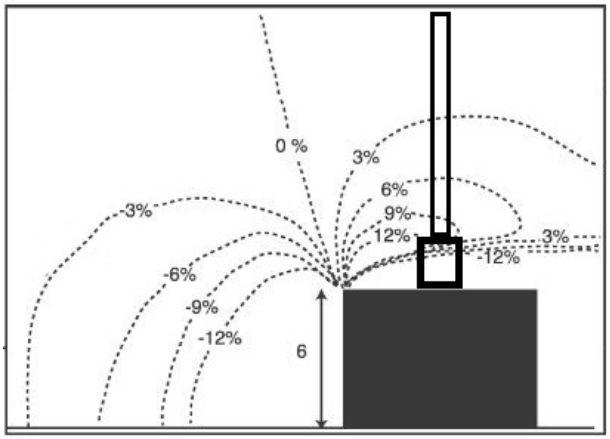

Figure 1.10: The horizontal flow field velocity distortion for a beam-on flow with a schematic representation of a Turbosail [17]

Another large effect, which differs from tests on land, is the fact that the ship is moving, so the apparent wind differs from the true wind in both strength and direction. This is depicted in Figure 1.11. Where the combination of the ship speed, the true wind speed and the true wind angle results in an apparent wind velocity with a corresponding angle.

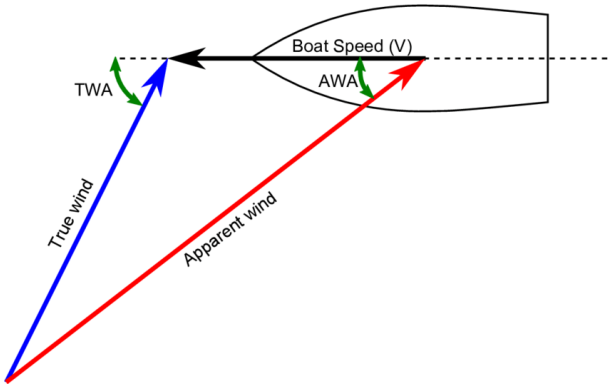

Figure 1.11: The definition of apparent wind

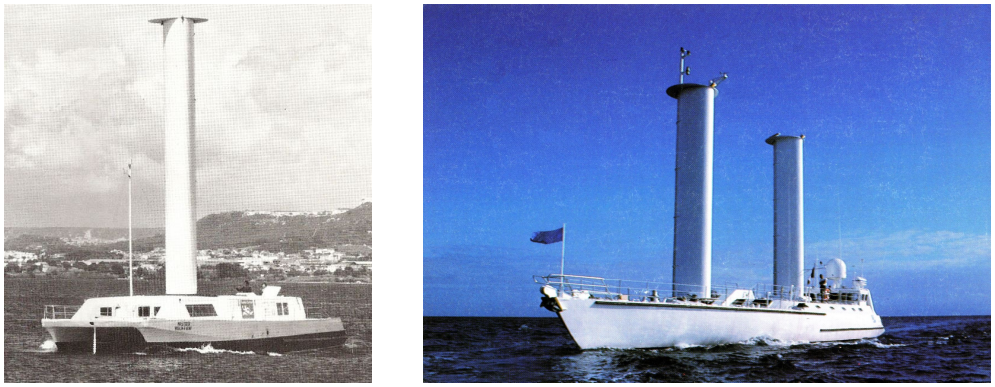

Figure 1.12: Left, the Moulin a Vent. Right, the Alcyone [4]

Figure 1.13: The Econowind measurement trailer

1.1.6. Existing prototypes

Several Turbosail prototypes have been built so far. The Cousteau foundation [4] has built two vessels, the Moulin a Vent and the Alcyone. At Econowind they have built a 5.5 meter Turbosail measurement setup on a trailer and a 40 foot container that contains two 11 meter high Ventifoil units.

The Moulin a Vent was the first sailing prototype delivered by the Cousteau foundation. And the Alcyone was the improved ship but equipped with two Turbosails. Both vessels are shown in Figure 1.12.

The measurement trailer of Econowind is made to gain insight into the behaviour of the Turbosail, which is called the 'Ventifoil'. This setup is shown in Figure 1.13. Various measurements and tests have been performed with this setup but despite all efforts the data was not available to the author, at the time of writing this thesis. The setup can rotate, has a fixed flap angle, a variable motor speed, a force measuring frame, three wind meters and one wind-direction meter. After fixing stability issues and malfunctioning sensors multiple measurements were performed to gain knowledge on the behaviour of the Ventifoil system. With the tell-tails attached and a smoke test it showed that, when enough suction supplied, the angle of attack can go up to 45 degrees without separation of the boundary layer.

The last prototype that will be described is the container unit of Econowind. This unit houses two 'Ventifoils' and is able to control, lift and lower them. The container unit (See Figure 1.14) can be mounted on the deck of a vessel and it is used at sea to collect data for improvement of the design and commercial purposes. With the first measurements Econowind claimed energy savings of 10 to 20 %[5]. This 11 meter prototype will be used in the results as a benchmark to compare other possible improved designs.

Figure 1.14: The container unit of Econowind

2

Literature Review

In this chapter the most important literature will be discussed in order to find the knowledge gap. First of all the report of the Cousteau foundation [4] will be discussed. Secondly the researches using wind tunnel test will be reviewed, followed by the CFD research. The goal is to find the literature gap which can be used to formulate a research question for this thesis.

2.1. Cousteau

The founder of the Turbosail is the French oceanographer Jacques-Yves Cousteau. Together with his associates he used Wind Assisted Ship Propulsion (WASP) with the goal to find a way to lower the emissions of their prototypes. They tend to achieve this goal by using their invention called the Turbosail. As mentioned in the previous chapter this was first applied on the Moulin a Vent and later at the special built Alcyone. Wind tunnel tests were performed to gain knowledge on the preferred shape and behaviour of the Turbosail. These results were compared to the analytical results to validate the calculations.

Another interesting section of this report [4] is the comparison with the Flettner rotor, which is one of the other WASP systems. The comparison is shown in Figure 2.1. The vertical axis represents the lift coefficient, in this figure C_L. On the horizontal axis the power coefficient is placed, the power coefficient is determined by Equation 2.1, where P_a is the required power for aspiration. For the Flettner rotor the power required for rotation is used. Four cases are considered, a circular Turbosail, an ovaloid Turbosail, a Flettner rotor with end-plates and a Flettner rotor without end-plates. The graduations marked on the curves of the Flettner rotors correspond to the ratio of peripheral speed of rotation to the speed of flow.

$$C_a = \frac{P_a}{\frac{1}{2}\rho A U_w^3} \tag{2.1}$$

It shows that for lift coefficients up to 6.8 the ovaloid Turbosail requires less power compared to both types of Flettner rotors and at a lift coefficient of 4 the ovaloid Turbosail uses only one third of the energy a Flettner rotor with end-plates would require [4]. But, at lift coefficients of higher than 6.8 both the circular Turbosail and the Flettner rotor with end-plates are performing at a lower power consumption. It must be kept in mind that this comparison does not include the drag coefficient.

This research also includes a simulation to investigate the economic feasibility. These findings together makes the "Fondation Cousteau and Windship Propulsion" a useful and founding report which opens possibilities for further research. After this research other researchers also discussed this subject.

2.2. Wind tunnel research

Wind tunnel research is an interesting method to test and measure the behaviour of a system, it is capable to capture all physics but the effects of the scaling of a model must be kept in mind.

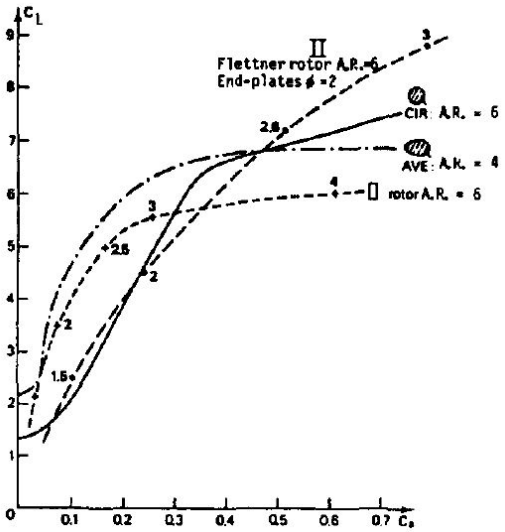

Figure 2.1: Comparison of the power necessary for the working of Flettner rotors and different Turbosail geometries [4]

One of the significant papers written is "Flow past a wind-assisted ship propulsion device" by H.T.Low et al.[15]. They systematically vary the geometry of a circular Turbosail in wind tunnel tests. Or as they stated: "One of the main objectives of the present study is to examine the effects of independent variations in the flap and suction locations." Interesting is the conclusion that the flap angle could deviate from its optimum as much as $\pm 20^\circ$ without adversely affecting the performance. Additionally, they found an optimum condition at a $C_q = 0.09$ where the lift coefficient is 4.2 and the lift to drag ratio is 6. This C_q is almost twice as high as the recommended C_q found by Cousteau. This could be due to the different shape, or the lack of considering the required energy for aspiration by Low.

Tsukasa Shiii et al.[22] also measured the performance of a Turbosail with a circular shape called C-pass (see Figure 2.2). They used a permeability of 40% and holes of 4mm and found an estimated maximum lift coefficient of 3.5. Which is low compared to the ovaloid Turbosail of Cousteau. The decrease of lift coefficient could be due to the exceptional large perforated area of the C-PAS. The tested models have a length of 149mm and a diameter of 60mm.

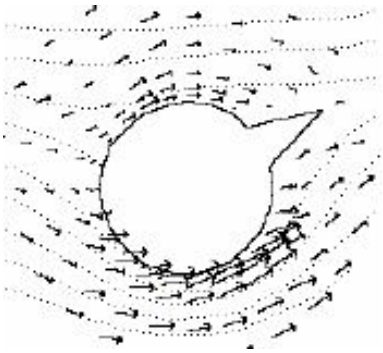

Figure 2.2: The flow around the C-PAS of Shiii et al. [22]

2.3. CFD research

Computational Fluid Dynamics (CFD) calculations are increasingly being used. This is because a CFD model has the advantage that parameters can easily be varied without the need of building a whole new scale model. However, it must be kept in mind that the assumptions and possible simplifications can influence the result of the simulation. The following paragraphs will describe some of the previously done researches on this subject.

Hcini et al.[7] developed an efficient numerical code for the prediction of the aerodynamic characteristics of a Turbosail. This model is verified and validated with the experimental data of Cousteau. Based on this research they did a profile analysis [8]. The model is used for the prediction of the aerodynamic effects of a Turbosail when varying the profile thickness, amount of suction and flap geometry. Concluded is that the primary effect of the flap is to increase the lift, while the main effect of the suction is to reduce the drag. But is must be kept in mind that these results are made with suction coefficients (C_q) of 0.0045 and 0.009. Which are very low compared to the coefficients used by Cousteau[4], where a coefficient of 0.047 is used.

O. Guerri et al.[6] did a numerical simulation that focussed on the Turbulent flow patterns and the shape of the flow separation around the profile. They modeled not only the outside of the Turbosail, but also a part of the inside as is shown in Figure 2.3. This is done by using slots as permeable surface and a cylinder as suction-pipe. Concluded is that it is unlikely that vibration issues due to vortex shedding will take place. This is due to the boundary layer suction which prevents the vortex shedding form occurring.

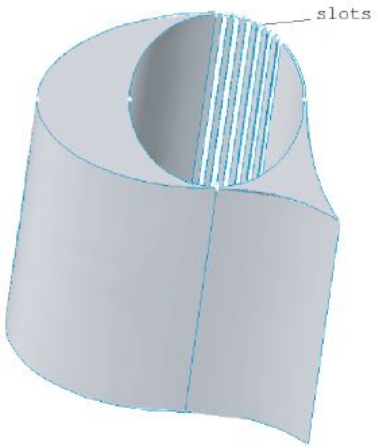

Figure 2.3: The model used by Guerri [22]

The theses written at the TU Delft are done by Anton Kisjes [12] and Laurens-Jan Lagendijk [13]. First Anton Kisjes made a Fuel Prediction Program (FPP) and CFD calculations on a given geometry to improve the FPP. This FPP is interesting due to the complexity of the system with the linkage with the hull and propulsion system and shows fuel savings of up to 20%.

Laurens-Jan Lagendijk performed systematic parameter variation CFD tests to find an optimal geometry. His finding is that the flap angle has a small effect on the performance, but increasing the length of the flap has a relatively large positive influence, which is in line with Hcini[8]. Also, an increase in thickness is found to be favourable. Interesting is the positive influence of placing the suction perforation more aft. Both authors state that more research is required into the suction system of the Turbosail.

2.4. Research question

As described in the previous sections, a lot of research is already performed on the Turbosail topic. Cousteau, Low, Shiii, Hcini and Kisjes all investigated the outer geometry. Guerri et al. have modeled the inside, but they did this by using slots and without a fan. Lagendijk has modeled the holes but, only a small segment that eliminates the possible influence of a non uniform suction distribution. The Turbosail is a propulsion device with the purpose to reduce the energy consumption of ships. With this purpose in mind, the importance of an efficient suction system is clear. More knowledge is required to be able to determine the performance of the current system and if possible to improve this system. Based on this information the aim and research questions can be stated.

The aim is to gain insight in the behavior of the internal suction system and its effect on the total system performance.

This aim can be translated in the following research questions:

1. How can the relation between the outside geometry, the inside geometry, the fan and the drive be described and modelled?
2. How sensitive is the total suction system for variations of different parameters?

The scope of this research is limited from the drive to the perforation holes. Detailed research of the behavior of the airflow outside the Turbosail is outside of the scope. In this research the total system performance is described by the energy required to provide a given volume flow through the perforated area of a Turbosail.

2.5. Approach & outline

With the aim, research questions and the scope stated the approach can be described. The function of the approach is to guide this research in order to answer the research questions.

1. The reality must be analysed to result in a conceptual model. To achieve this a sufficient type of modeling must be chosen.
2. The conceptual model must be programmed to result in a computerized model. This must be done in a manner that parameters of the wing and fan can be varied easily.
3. The computerized model must be verified to ensure the mathematical correctness.
4. The possible calibration and validation procedures, that are required to incorporate measurements into the research at a later stage, must be described.
5. Results can be calculated with the verified model in order to gain insight in the sensitivity of different parameters.

The first two steps will be discussed in Chapter 3: Model theory & implementation. The model verification is shown in Chapter 4. The suggested calibration and validation is shown in Appendix A. And finally the results are described in Chapter 5 finishing with the Conclusions & Recommendations in Chapter 6.

3

Model theory & implementation

The first step is to select a type of modeling to be able to make a simple but sufficiently extensive model of the inside of a Turbosail. Basically this can be seen like a pipe flow system with holes aspirated by a fan. The model can be made using a lumped parameter approach or using CFD. Choice is made to use a lumped parameter approach. This is because of the straightforward implementation of the characteristics of an existing fan. The model is created in Matlab Simulink. This chapter describes the foundation and construction of this model.

The model consists out of an array of elements and a fan, as is shown in Figure 3.1. The advantage of this model is that the number of elements can easily be changed to reach a favorable resolution. The elements consists out of a Volume (V) and a resistance element (Rhole or Rh for the hole resistance and Rpipe or Rp for the pipe resistance). The fan part consist out of a fan, a motor and a controller. In the coming subsections these parts will be discussed.

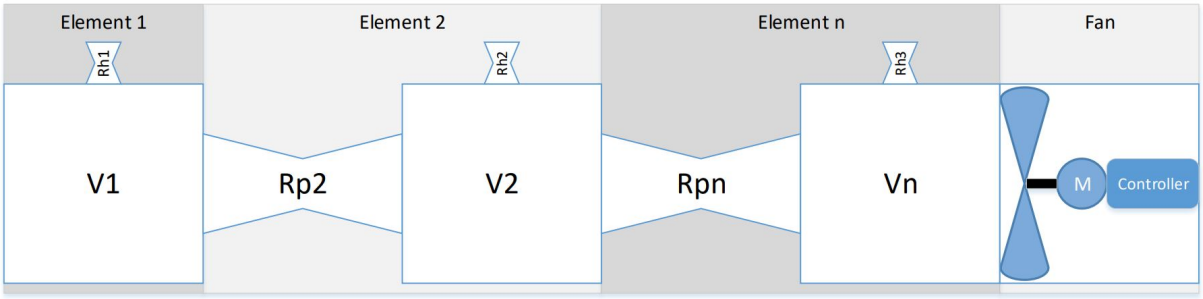

Figure 3.1: The basis layout of the model

3.1. Model theory

The foundation of making the model consists of a combination of differential and algebraic equations, based on the lecture slides of Stapersma [23] where required alternatice formulations are used.

3.1.1. Volume

The volume part of the element calculates the pressure inside the volume using the difference in incoming and outgoing mass. This is shown in Figure 3.2. The first equation is the mass balance stating that when there is no change in mass the incoming mass must equal the outgoing mass, see Equation 3.1.

$$\frac{dm}{dt} = \dot{m}_{in} - \dot{m}_{out} \tag{3.1}$$

This difference in mass flow must be integrated to determine the in- or decrease of mass inside the volume. After this integration the mass is divided by the volume of the element, so the density of the medium inside the volume is obtained (See Eq. 3.2).

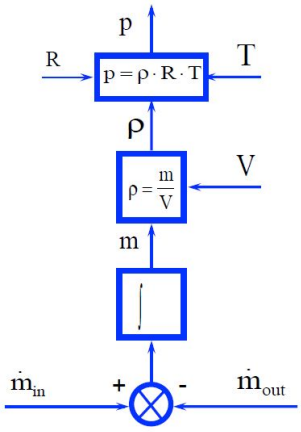

Figure 3.2: The volume part of the element

$$\rho = \frac{m}{V} \tag{3.2}$$

The ideal gas law is stated in Equation 3.3 and is used to calculate the pressure inside the volume, where R is the gas constant. The ideal gas law is assumed to be sufficient for this purpose due to the stability of air at the used temperatures and pressures.

$$p = \rho RT \tag{3.3}$$

With this volume part the pressure is calculated based on the difference of the incoming and outgoing mass. The medium, air in this case, is assumed to behave like an ideal gas. This assumption is made due to the fact that the temperature will not change significantly and the changes in pressure are relatively small. The next subsection will discuss the resistance part of the element.

3.1.2. Resistance

The resistance part of the main element consists out of an inertia part and a pressure loss part. The main element has a pipe resistance part (Rp) and a hole resistance part (Rh). The pipe resistance part represents the resistance through the Turbosail itself and the hole resistance represents the resistance through the perforated area corresponding with that specific element.

First the inertia part is considered (See Figure 3.3). This part is equal in both Rp and Rh. The pressure difference is used as input to compute the mass flow through the element. This is shown in Equation 3.4.

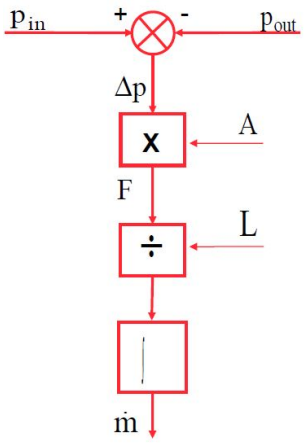

Figure 3.3: The inertia part of the element

$$\frac{d\dot{m}}{dt} = \frac{(p_{in} - p_{out})A}{L} \tag{3.4}$$

This equation is a combination of Euler's momentum balance (Eq. 3.5) and the definition of momentum (Eq. 3.6).

$$\frac{d(mv)}{dt} = (p_{in} - p_{out})A = F \tag{3.5}$$

$$mv = \rho ALv = \dot{m}L \tag{3.6}$$

The next step is to develop the pressure loss part. This part is shown in Figure 3.4. The pressure loss must be calculated with the mass flow used as input.

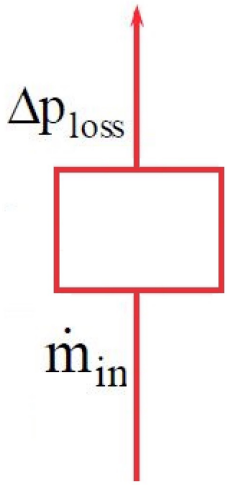

Figure 3.4: The pressure loss part of the element

First the pressure loss part of the inside of the Turbosail (Rp) is discussed. For this model the assumption is made to consider the intersection of the Turbosail as a circle with diameter D. The common pressure loss calculations have two possibilities, one for laminar flow and one for turbulent flow. Both are discussed below[10].

The pressure loss is described by:

$$\Delta p_{loss} = \zeta \frac{1}{2} \rho v^2 \tag{3.7}$$

where for laminar flow the pressure loss coefficient zeta ζ is

$$\zeta = \lambda \frac{L}{D} \tag{3.8}$$

and the Darcy friction factor λ for laminar flow is

$$\lambda = \frac{64}{Re_D} \tag{3.9}$$

and for turbulent flow λ is

$$\lambda = \left(-1.8 \log \left[\frac{6.9}{Re_D} + \left(\frac{Ro}{3.7} \right)^{1.11} \right] \right)^{-2} \tag{3.10}$$

with

$$Re_D = \frac{\rho v D}{\eta} \tag{3.11}$$

and

$$Ro = \frac{k}{D} \tag{3.12}$$

for laminar flow this yields

$$\Delta p_{loss,lam} = \zeta \frac{1}{2} \rho v^2 = \frac{64}{Re_D} \frac{L}{D} \frac{1}{2} \rho v^2 = \frac{32 L \eta}{D^2} v \tag{3.13}$$

and for turbulent flow

$$\Delta p_{loss,tur} = \zeta \frac{1}{2} \rho v^2 = \frac{\lambda L \rho}{2D} v^2 \tag{3.14}$$

The choice between these two pressure loss calculation formulas depends on the fact whether the flow is turbulent or not. This is expressed by the Reynolds number. The Reynolds number can be calculated using equation 3.11, where for air the density is $\rho = 1,293 \frac{kg}{m^3}$, the kinematic viscosity is $\eta = 15.11 \cdot 10^{-6} \frac{m^2}{s}$ and the average diameter at the inside of the Turbosail is set at $D = 1m$. This results in a Reynolds number of $Re_D = 3,3 \cdot 10^5$, which is considered as turbulent flow. For this reason Equation 3.14 is used to calculate the pressure loss for Rp.

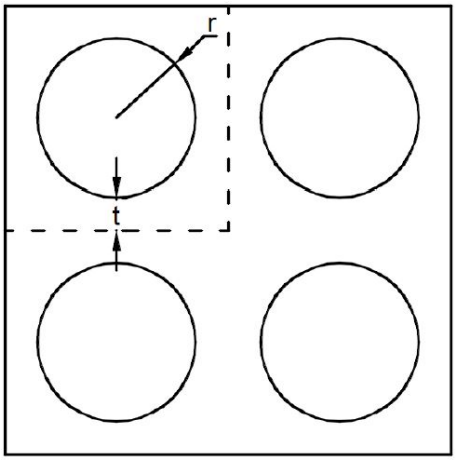

Figure 3.5: Holes distribution[13]

$$t = \frac{1}{2} \left(\frac{\sqrt{\pi}}{\sqrt{\kappa}} - 2 \right) r \tag{3.15}$$

$$\kappa = \frac{A_0}{A_1} \tag{3.16}$$

Now the pressure loss through the hole part (Rh) can be described. The hole part is in fact a perforated surface what can be describes using Figure 3.5. In this figure a segment of the perforated plate is seen and the shape is described using the radius (r) of the hole and the width of the edge (t), the corresponding formula to calculate the distance between the holes is shown in Equation 3.15. In this formula a clear relationship between the κ, r and t is shown. Where t is in this case the half of the distance between neighbouring holes. Another way to describe this shape is by using the hole diameter and permeability κ (see Eq. 3.16). Where A_0 is the area of the hole and A_1 is the area of the square segment. The width of the perforated plate can be calculated by Equation 3.17.

$$w_{perforation} = N_{Holes} \frac{\left(\frac{\sqrt{\pi} D}{2\sqrt{\kappa}} \right)^2}{L_{Turbosail}} \tag{3.17}$$

Up to this date there are difficulties encountered with determining the flow resistance through a perforated plate. For this model the Handbook of Hydraulic Resistance[11] is used. Known is that this formula will not give a perfect representation of the problem, but the deviation might get clear when validating the model. The pressure drop is calculated by formula 3.18. This formula can be used for a perforated plate with sharp, thick edged orifices with a flow perpendicular to the surface.

$$\zeta = \frac{\Delta p}{\frac{\rho v_0^2}{2}} = \left(0.5 + (1-\kappa)^2 + \tau(1-\kappa) + \lambda\frac{l}{D}\right)\frac{1}{\kappa^2} \tag{3.18}$$

To cope with the fact that the flow velocity at the perforation is not perpendicular to the surface and literature on this specific subject is lacking, an adjustment in the method is required. For now an estimation of the flow resistance of this part is made by multiplying the flow-resistance through a perforated plate with a constant times the wind velocity squared. This constant needs to be found by calibration tests. To be able to compute in an earlier phase than after the calibration, decision is made to use a value determined by the following method: The projection for the flow trough the hole is an oval, for now the simplification is made to account for the smaller projected inlet hole by multiplying ζ of equation 3.18 by a factor of 1.2.

The permeability κ is set at 0.4 to maintain similarities with the thesis of L. Lagendijk[13]. Due to the fact that κ is of great influence on the flow resistance the decision has been made to vary the amount and the diameter of the holes while maintaining a constant κ by changing the width of the perforated plate. In the calibration phase of the model this value can be used to tune the model to comply with the prototype. λ is set at 0.015 and τ is interpolated, both according to the available information as found in the Handbook of Hydraulic Resistance[11].

The general resistance part, with the inertia and resistance part, is shown in Figure 3.6 this combination is applicable for both Rh and Rp. The equivalent of one total element (the volume part and two resistance parts coupled) is shown in Figure 3.7. Where the left resistance element is the Rh, the middle resistance element is the Rp and on the right the volume element is seen.

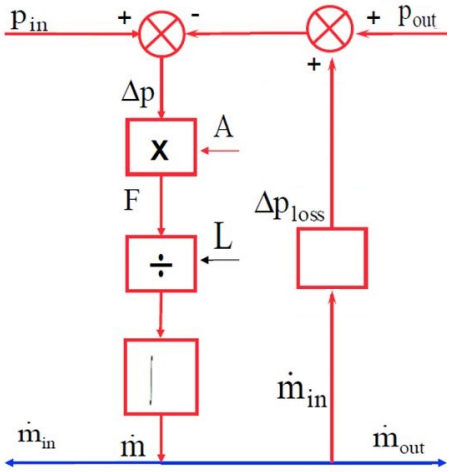

Figure 3.6: The general resistance part

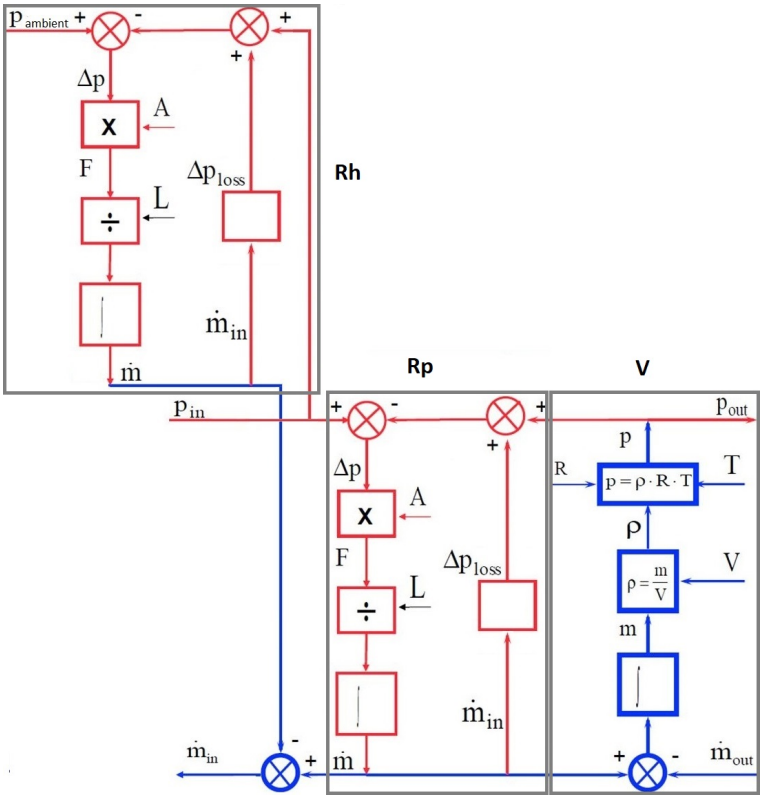

Figure 3.7: The total element

The first element on the non-fan side, contains as mentioned earlier and depicted in Figure 3.1 only a volume and hole resistance part. This is shown in Figure 3.8. Where the left red part is the resistance part of the hole and the right blue part is the corresponding volume element.

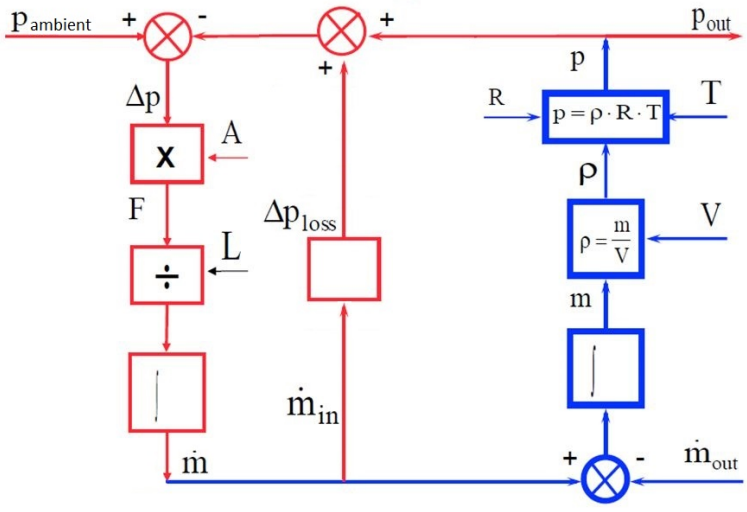

Figure 3.8: The first element

3.1.3. Fan system

The fan system consists out of a fan, a motor and a controller. This section will describe the theory used to model the fan system. To implement a realistically operating fan into the system a dimensionless fan representation is preferred. In order to be able to easily differ the fan power and scale the size of the system. To model this, the dimensionless pressure and dimensionless volume flow is used as stated by E.N. Lightfoot et al.[14]. Equation 3.19 is used to calculate the dimensionless pressure difference. This dimensionless pressure difference is used to find the corresponding dimensionless volume flow using equation 3.20. To find the right dimensionless volume flow using the dimensionless pressure difference specific fan information is required. The model layout is shown in Figure 3.9.

$$\pi_2 = \frac{\Delta p}{\rho \omega^2 D^2} \tag{3.19}$$

$$\pi_1 = \frac{Q}{\omega D^3} \tag{3.20}$$

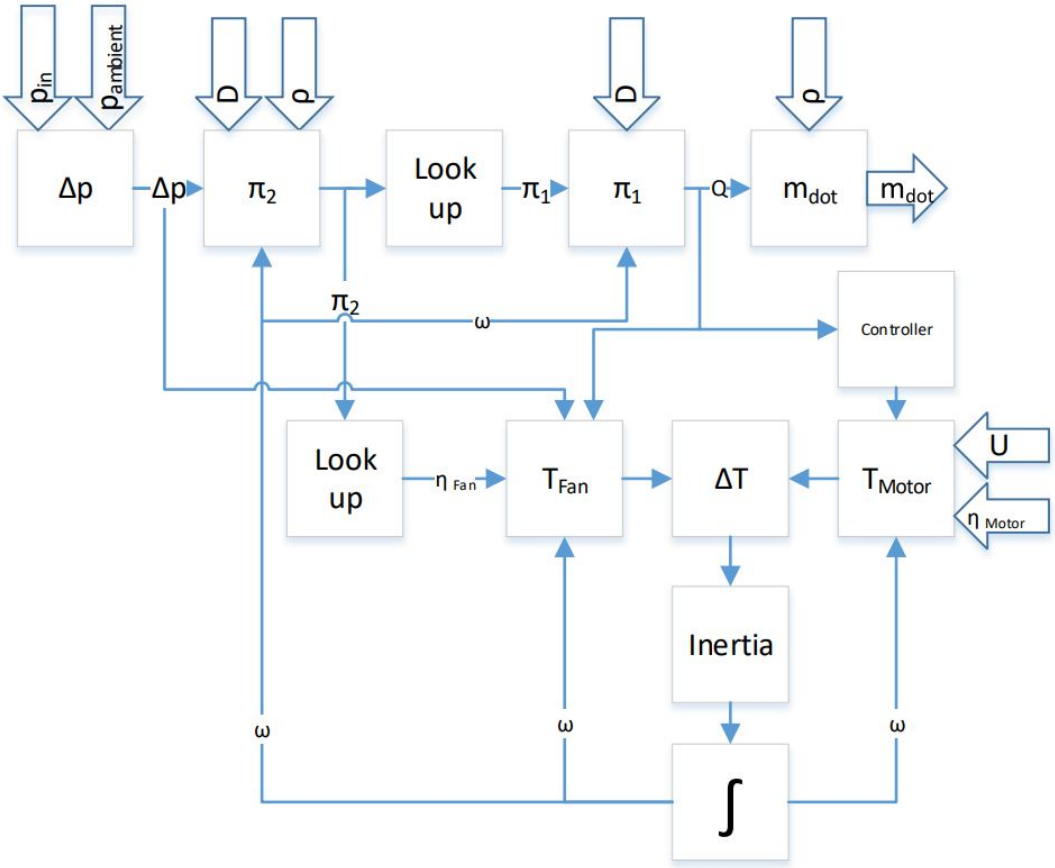

Figure 3.9: The first element

The fan torque must be calculated to be able to determine the required motor power. Equation 3.21 is used to calculate the required fan torque. Where η_{Fan} is the efficiency of the fan. This fan efficiency is fan specific and can be linked to the dimensionless pressure π_2.

$$T_{fan} = \frac{Q \Delta p \omega}{\eta_{Fan}} \tag{3.21}$$

The torque of the motor can be calculated with the rotational speed, the power consumption and the motor efficiency (Eq. 3.22). Where η_{Motor} is the motor efficiency, U is the motor voltage and I is the electrical current.

$$T_{Motor} = \frac{UI}{\omega \eta_{Motor}} \tag{3.22}$$

The resulting torque, when the fan torque is subtracted from the motor torque, is used to calculate the fan acceleration (See Eq. 3.23). Where J is the rotational inertia and $\frac{d\omega}{dt}$ is the rotational acceleration. When $\frac{d\omega}{dt}$ is integrated the rotational speed ω of the fan is obtained. With the calculated ω the feedback loop can be closed.

$$\frac{d\omega}{dt} = \frac{T}{J_{Fan} + J_{Motor}} \tag{3.23}$$

The last missing part is the controller. The controller has the function to drive the electric motor so that the requested performance will be delivered. In this theoretical case a PI controller that uses the requested C_q as desired value is assumed to be sufficient.

3.2. Geometric description

The value of the model is the possibility to make the geometric properties comply with the Turbosail that are aimed to be assessed. The model is divided in elements. This yields Equation 3.24 for the length per element.

$$L_{Element} = \frac{L_{Turbosail}}{N_{Elements}} \tag{3.24}$$

The same situation applies to the amount of holes per element. This is shown in Equation 3.25.

$$N_{Holesperelement} = \frac{N_{Holes}}{N_{Elements}} \tag{3.25}$$

The ovaloid shape of the Turbosail is simplified by using a circle. This means that only the diameter of the circle is necessary to describe the area at a certain position. This simplification is also made by O. Guerri [6].

The taper is defined in a percentage. Where 10% taper gives an increase of 10% at the diameter of the pipe at the fan side. The rest of the pipe is scaled in such a way that the total pipe volume does not change and the decrease in diameter over the length of the pipe is linear.

Other more straightforward parameters required for the simulation are the plate thickness of the Turbosail, κ and the hole diameter where the width of the perforated plate is calculated using Equation 3.17.

3.3. Model implementation

With the knowledge of the previous section a model can be made using Matlab Simulink. This is done by making a basic model part, the earlier described main element, which Matlab uses to build the model with the defined parameters. The parameters that can be varied are: length, diameter, number of holes, temperature, wall thickness of the tube, hole diameter, taper, the ambient pressure and the fan characteristics. In this way it is possible to create a set of different systems with minimal effort.

The model can be divided, as described in the previous section, into two main parts. One is a series of elements which models a perforated pipe and the other part is a fan. In Matlab Simulink this yields Figure 3.10 where the first three elements models the pipe and where the last subsystem models the fan. In the next subsections both parts of the system will be discussed.

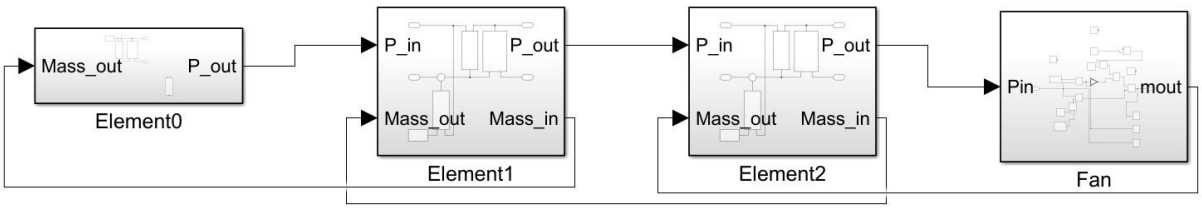

Figure 3.10: The model with three elements

3.3.1. The perforated pipe

The perforated pipe is made out of a series of elements which all contain the lumped parameter model mentioned in section 3.1. The first part discussed is the volume element. The implementation in Matlab Simulink is shown in Figure 3.11. The green parts are "to Workspace" parts and are used to transfer data out of the Simulink environment into the Matlab environment.

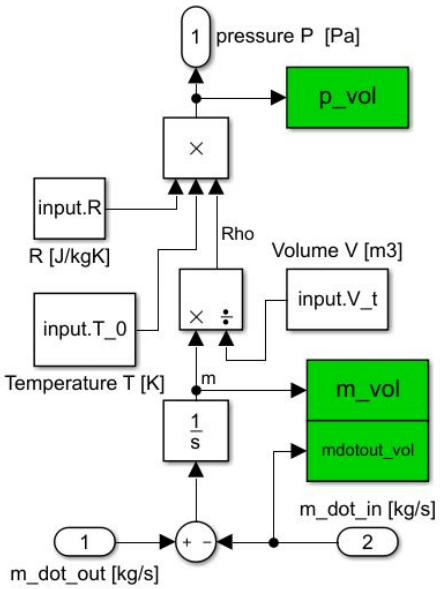

Figure 3.11: Volume element

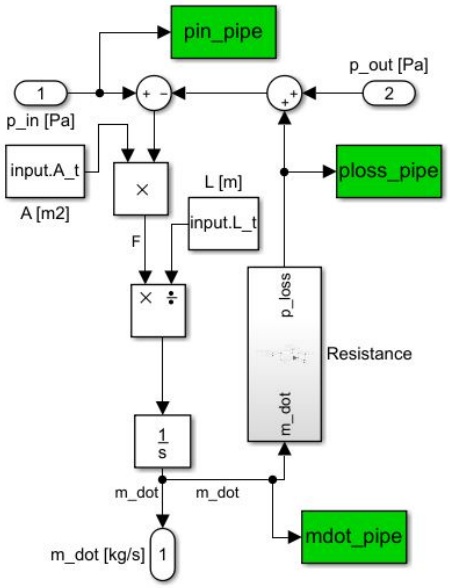

Figure 3.12: Pipe resistance element

Now both resistance parts can be discussed, starting with the pipe resistance element. In Figure 3.12 it can be seen that the left part represents the earlier mentioned inertia part and the right part represents the resistance part. The pressure loss part is shown in Figure 3.13. The pressure loss for the pipe is calculated using the Darcy friction factor. This is modeled as is shown in Figure 3.14.

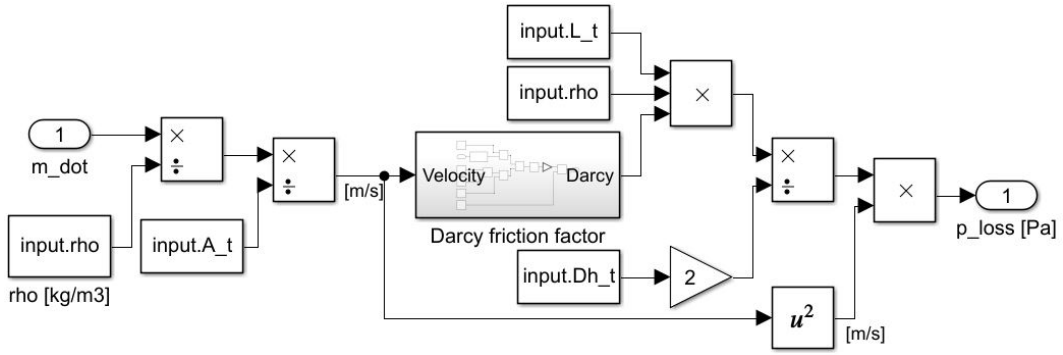

Figure 3.13: Pipe pressure loss

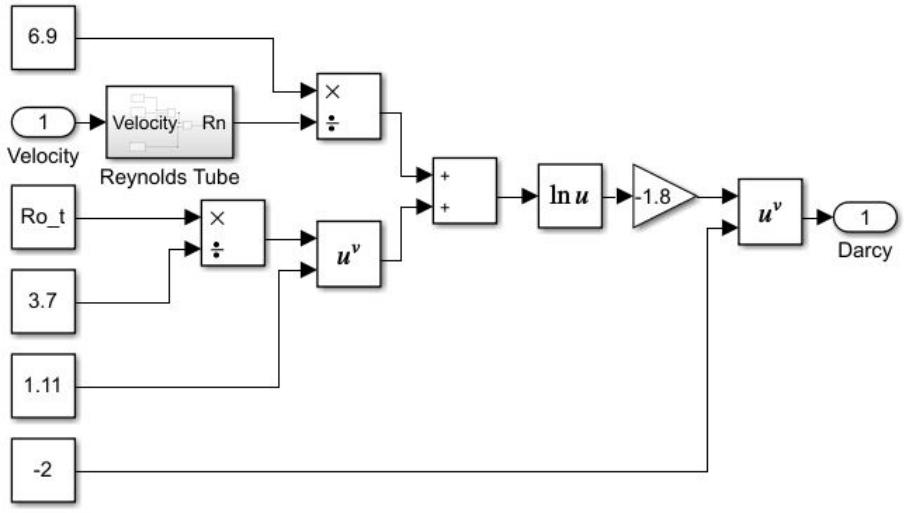

Figure 3.14: Darcy friction factor

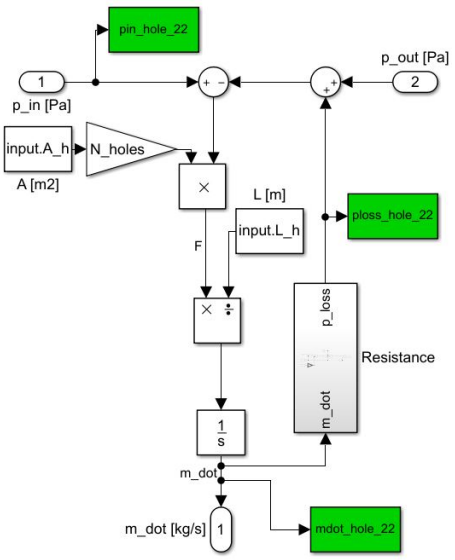

Figure 3.15: Hole resistance element

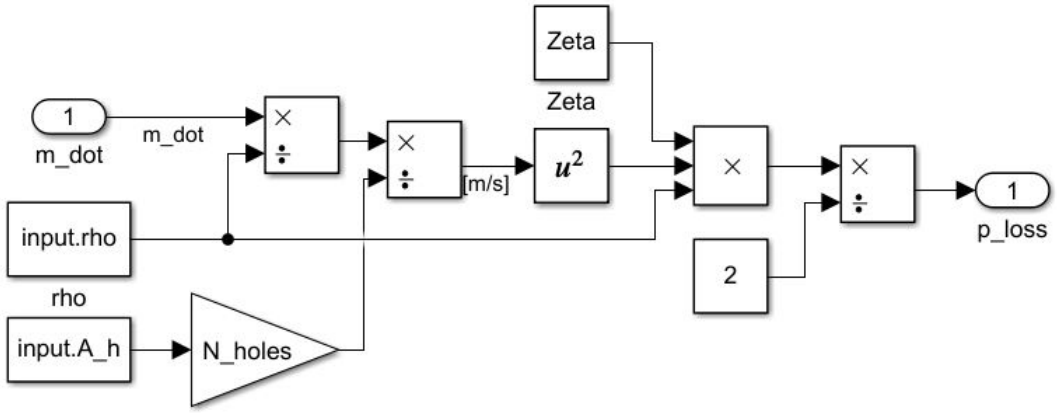

Figure 3.16: Hole pressure loss

The last part to implement in Matlab Simulink is the hole resistance element. This element is shown in Figure 3.15 and consists just as the pipe resistance element out of two parts, a inertia part and a pressure loss part. Note that the hole area in the inertia part (left) is multiplied by the amount of holes to retrieve the total hole area of that particular element. The right part consists out of the resistance part. This resistance part is shown in Figure 3.16. Where again the hole area is multiplied by the amount of holes and the Zeta (ζ) is calculated in Matlab using Equation 3.18.

These parts combined together form the main part, this main part can be seen in Figure 3.17. The connection between the different parts comply with the model made in the previous section. The first element consist only out of a volume and a hole element (see Figure 3.18).

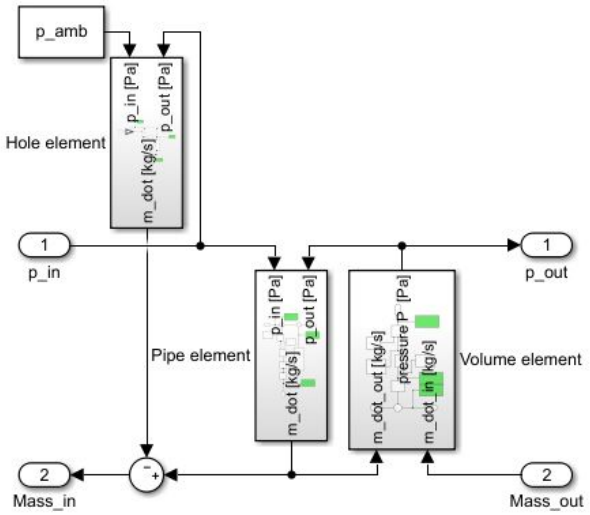

Figure 3.17: The main element of the model

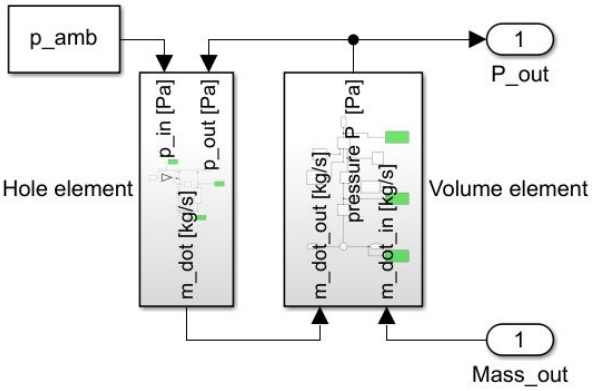

Figure 3.18: The first element of the model

3.3.2. Fan

At the other side of the element series the fan system element is placed. This fan system element receives, as mentioned before, a pressure difference and a requested C_q and it gives the corresponding mass flow using the characteristics of the fan and the settings of the controller. The fan model made in Matlab Simulink is shown in Figure 3.19. The lookup tables are both based on specifications of the the ALMECO ADK A1.001.442 Short Case Fan [1]. This forms the relations between pressure, volume flow and efficiency to be similar to this type of fan. This fan is comparable in size and power with the type of fan used in the Econowind container unit.

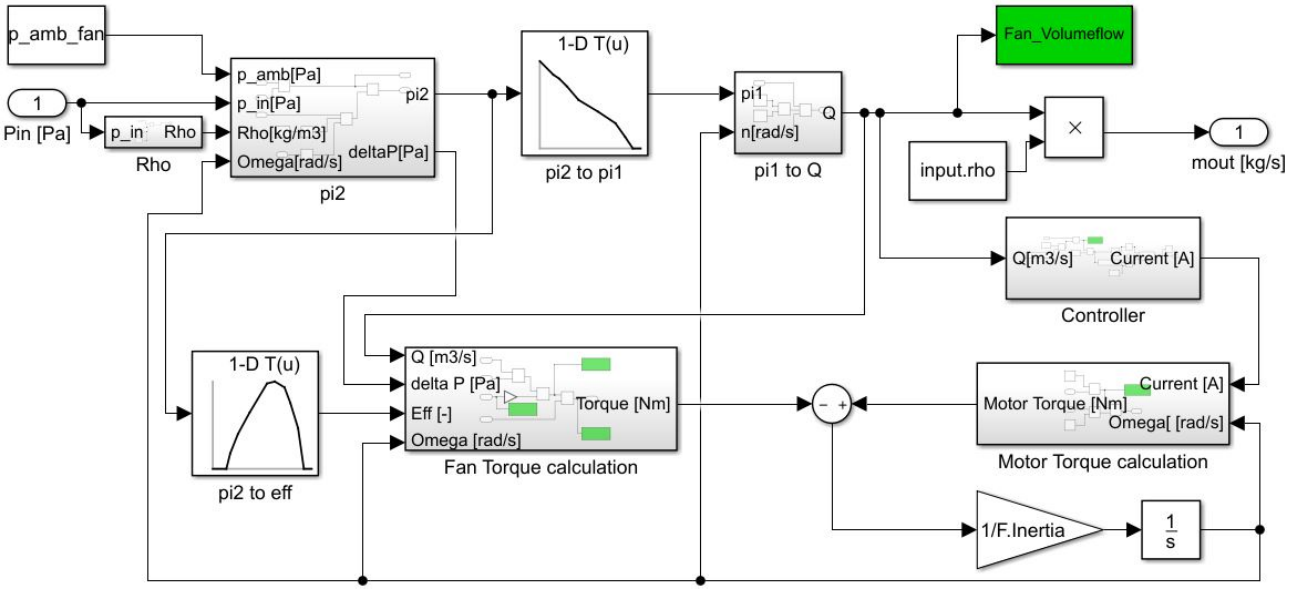

Figure 3.19: The fan of the Matlab Simulink model

Different starting issues were encountered while modeling the fan. In both lookup tables there were problems with the starting sequence because of the extreme input values which caused the system to extrapolate, which resulted in negative values. To solve this problem decision is made to flatten out the extreme values of the look-up tables. This will result in the output not turning negative and the system will maintain its stability. When simulating the model it must be kept in mind that there can be a situation where the fan is operating at these extreme values, in that case the output is not realistic. Another issue is that the system will encounter an error when the rotational speed is zero, this happens due to the fact that it will introduce a divide by zero problem and it is solved by introducing a initial rotational speed integrator value of 0.1. The last main issue is a numerical starting stability issue with the interaction of total pipe system, this is solved in the controller.

The controller consists out of a PI controller which is driven by the difference between the current C_q value and the requested C_q value and delivers the required current to be able to reach the requested C_q. To solve the starting stability issues decision is made to use a starting peak for the first 0.1 seconds.

3.4. Operating conditions

Operating conditions have to be chosen to start the simulation. The wind speed is set at $U_w = 5.67 m/s$ as found by L. Lagendijk[13] by calculating the most occurring wind speed in the Baltic and North Sea area. Although $U_w = 5.67 m/s$ is the most occurring wind speed, L. Lagendijk found that to obtain maximum performance of the Turbosail an energy density spectrum analysis is required, after which he concluded that the mean of the energy density spectrum is at $U_w = 10.8 m/s$. These two wind speeds will be used in the simulation. The wind direction will not be varied.
The suction coefficient is set on $C_q = 0.047$ as found as optimal value by Cousteau[4] and the projected wing area is $A = 11 m^2$ corresponding with the Econowind container unit. The ambient pressure is set on $10 \cdot 10^4 Pa$ and will be used as pressure at the outside of the perforation.

4

Verification

The verification, calibration and validation processes are of great importance to assess the correctness and usefulness of a model. In this chapter the verification will be performed and discussed for the suction model of the Turbosail as has been described in the previous chapter.

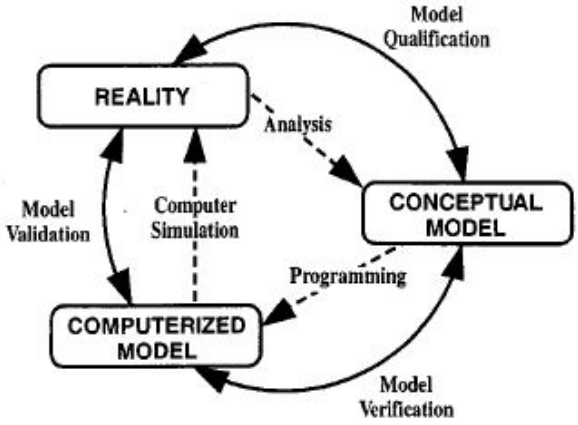

Figure 4.1: The development cycle as made by Schlesinger et al.[21]

The development cycle of a simulation model as depicted in Figure 4.1 is a good representation of the process of developing a computerized model. It shows the interconnection of the different aspects of this cycle. First the reality is analyzed to create a conceptual model. This conceptual model follows from a model qualification to ensure it is able to provide an acceptable level of agreement with reality. This phase already has been executed in Chapter 3.
The next phase is the programming of the computerized model. This is also fulfilled in Chapter 3 by implementing the analytic equations into a Matlab Simulink model. The following step depicted in Figure 4.1 is the computer simulation. However, to be able to have a better fit with reality the decision has been made to perform a calibration step between the verification and validation sequence. The required calibration and validation are described in the appendix.

The verification starts with a convergence study, intended to gain insight in the number of elements required. The second part of the verification chapter is the verification itself. This verification has the aim to test the mathematical correctness of the model.

Figure 4.2 shows the definition of the length of the Turbosail model. In this figure the holes are depicted as blue dots and the fan is visible on the right. This definition is used throughout the rest of this paper.

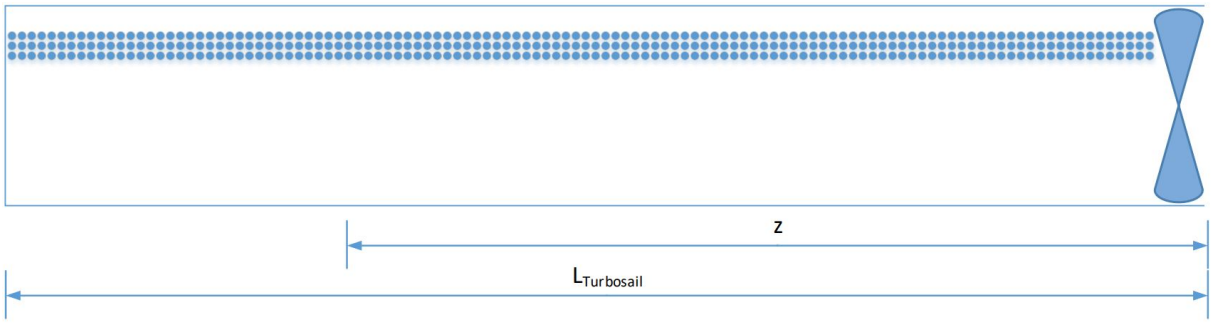

Figure 4.2: The length definition of the model
Table 4.1: Verification, the fixed parameters

$L_{Turbosail}$ [m]	Diameter [m]	Taper [-]	Number of holes [-]	κ [-]	C_q [-]
10	1	0	2000	0.4	0.047

Table 4.2: Verification, the varied parameters

Test	N-elem.[-]	Hole D [mm]	Wind vel. [m/s]	Density ρ [$\frac{kg}{m^3}$]	Kin. Visc. η [$\frac{m^2}{s}$]	$w_{perf.}$ [m]
Conv.	5-201	25	5.67	1.293	$15.11 \cdot 10^{-6}$	0.245
1	50	25	10.8	1.293	$15.11 \cdot 10^{-6}$	0.245
2	50	25	10.8	1.293	$15.11 \cdot 10^{-6}$	0.245
3.1	50	20	10.8	1.293	$15.11 \cdot 10^{-6}$	0.157
3.2	50	15	10.8	1.293	$15.11 \cdot 10^{-6}$	0.088
4	50	25	10.8	1.228	$15.11 \cdot 10^{-6}$	0.245
5	50	25	10.8	1.293	$15.11 \cdot 10^{-4}$	0.245

The parameters used in this chapter are defined in Table 4.1 and Table 4.2. The first table shows the parameters that are fixed throughout the verification process until Section 4.3. The second table shows the parameters that are varied in order to perform the verification.

4.1. Convergence study

The first step of the verification process is to obtain insight in the amount of elements necessary to be able to compute a valuable simulation. This is done with a convergence study. The advantage of a high number of elements is the high resolution that is obtained. But, this will increase the computational time. So a compromise must be made between resolution and computational time. First it has to be made clear why it is necessary to have more than one element. This is necessary because the pressure and flow difference over the length of the Turbosail has to be captured in order to gain insight into the flow behaviour of the inside of the Turbosail. And when only one element is used this will be uniform. The convergence test is done by varying the amount of elements while maintaining the same geometry. This study will result in the knowledge of what amount is sufficient for these tests and this result will be used in the rest of the verification and in Chapter 5.

The convergence study is done for a Turbosail with a length of 10 meter, a diameter of 1 meter, no taper, a κ of 0.4, 2000 holes of 25 mm in diameter and a wind speed of 5.67 m/s. The results of the convergence study are shown in Figures 4.3, 4.4 and 4.5. The first figure shows the distribution of mass flow per hole of ten different amounts of elements that are used to simulate the same situation. The lowest number of elements is 5, the highest is 201. It is clearly visible that the 5 element version is very coarse and when the number of elements increases the results refine.

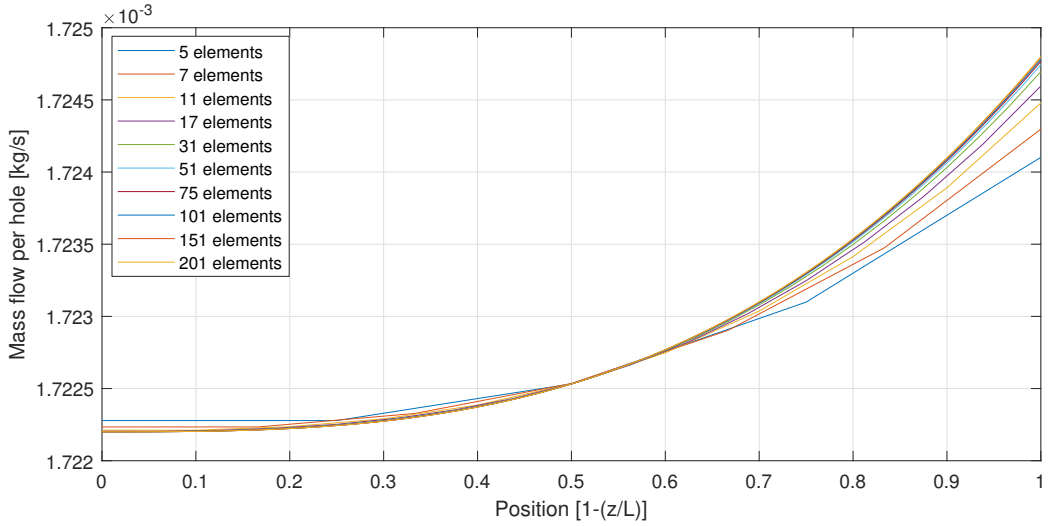

Figure 4.3: The behaviour of the mass flow per hole of different element resolutions over the length of the wing

To gain more insight in the situation three positions are chosen to take a closer look at. In Figure 4.4 the convergence of the first (top), middle and last (bottom) element are depicted. The 201 element computation is estimated as fully converged value and is set as 100%. It shows that all three positions do converge to a certain value. Clear is that the last element, which is the bottom one at the fan side, has the largest deviation. But it is still only a difference of 0.04%.

When the rotational speed of the fan is considered, Figure 4.5 indicates that the difference between the highest and lowest amount of elements is only 0.025%, which is also very small. It can be concluded that there is convergence, but the effect of choosing between a high or low amount of elements is small.

The goal of the model is to capture the flow behaviour over the length of the Turbosail. This is to be able to investigate the influence of changes in parameters like for instance the hole size, the amount of holes or the taper. Expected is that these changes in parameters may have an effect on the flow distribution, but the magnitudes of these effects are not known yet. With this in mind, the highest resolution is chosen with a computational time that is acceptable for the amount of tests that have to be performed. This results in a model with 50 elements, what is expected to be sufficient to capture the effects of the changes in parameters.

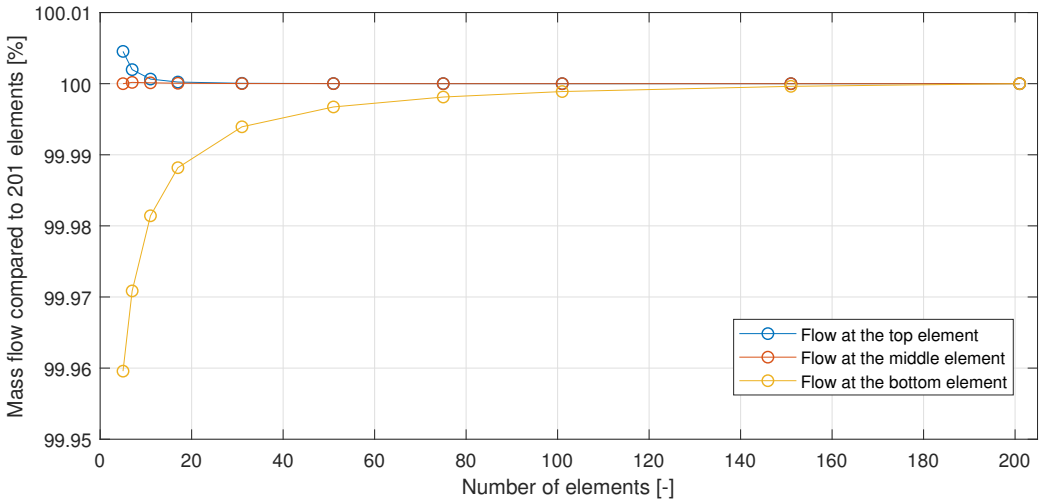

Figure 4.4: The convergence of mass flow through the left, middle and right hole

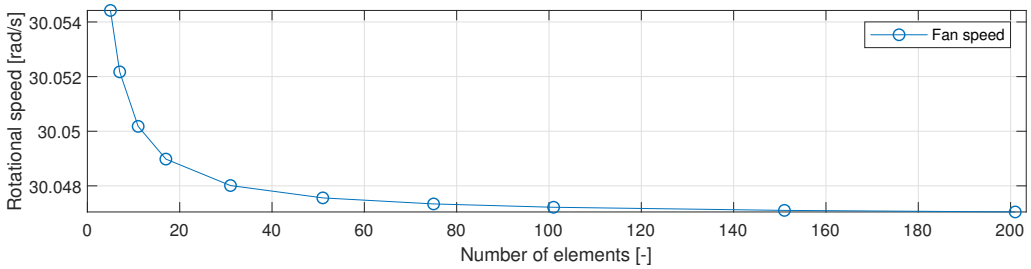

Figure 4.5: The convergence of the fan speed

4.2. Verification of the pipe flow system

"Verification: The process of determining that a computational model accurately represents the underlying mathematical model and its solution." [18]

The following part of the verification process is to test the mathematical correctness of the model. This is done by performing a number of carefully chosen tests in order to be able to assume the model as mathematically correct. This correctness is an assumption due to the fact that the amount of tests that could be done is theoretically unlimited. But with that statement the model will never be fully verified. The following five statements are defined to test the sensitivity of different parameter settings of the model.

1. The incoming and outgoing mass must be equal when operating in steady state
2. The flow per hole must increase when moving closer to the fan
3. The required pressure difference must be higher at an equal C_q when the holes diameter is decreased
4. Decreasing the air density must decrease the pressure difference
5. Increasing the kinematic viscosity must increase the pressure difference

The first test is comparing the incoming mass-flow with the outgoing mass-flow in steady state. For steady state the incoming mass must be equal to the outgoing mass (Eq.4.1).

$$\sum mass_{out} = \sum mass_{in} \tag{4.1}$$

This test is performed with the 50 elements version of the convergence tests and with a wind speed of 10.8 m/s. The sum of the incoming flow through the holes was $6.5633 \frac{kg}{s}$ and the outgoing flow through the fan was $6.5633 \frac{kg}{s}$. These are equal values, which means that the model passed this test successfully.

The second test is to check if a logical trend does occur in the model. The total flow resistance of each hole is a sum of the hole resistance and the series of pipe-resistances in front of it. The pipe resistance is compared

to the hole resistance very small which causes the total resistance of a path from the fan to a hole to increase slowly at increasing distance from the fan. This increasing resistance should cause a decreasing flow per hole at increasing distance from the source. The result of this verification test is shown in Figure 4.6. The increase in flow through the holes and a decrease in pressure in the pipe is clearly visible, although the effect is small. The model has passed this test because the expected trend does occur.

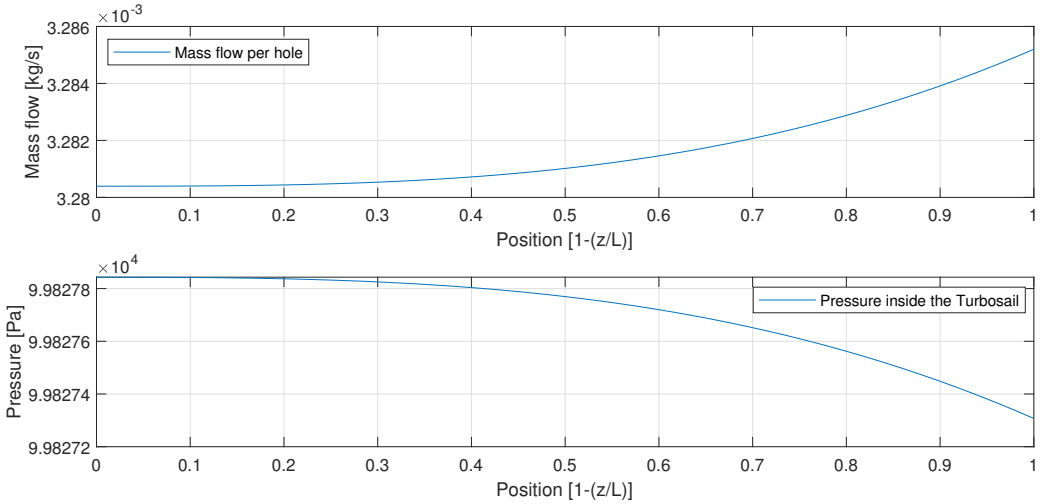

Figure 4.6: The second verification test shows a increasing flow through the holes and a decreasing pressure closer to the fan

The third test is to check when the hole-size is reduced that the pressure difference required to maintain the same C_q will increase. This is because the total resistance will increase and thus the required pressure difference must be higher to achieve the same C_q. The κ is fixed at 0.4 in these tests and the distribution of holes over the length is fixed. So the width of the perforated plate is decreased.

Three different situations are considered for this test: the baseline with holes of 25mm in diameter, one simulation with holes of 20mm and another simulation with holes of 15mm. In Figure 4.7 the results can be seen. When comparing these three situations it can be seen that the pressure is lower (thus a higher pressure difference is required) for the situations where the hole size is decreased. This effect is as expected, thus it can be stated that the model has passed this test successful.

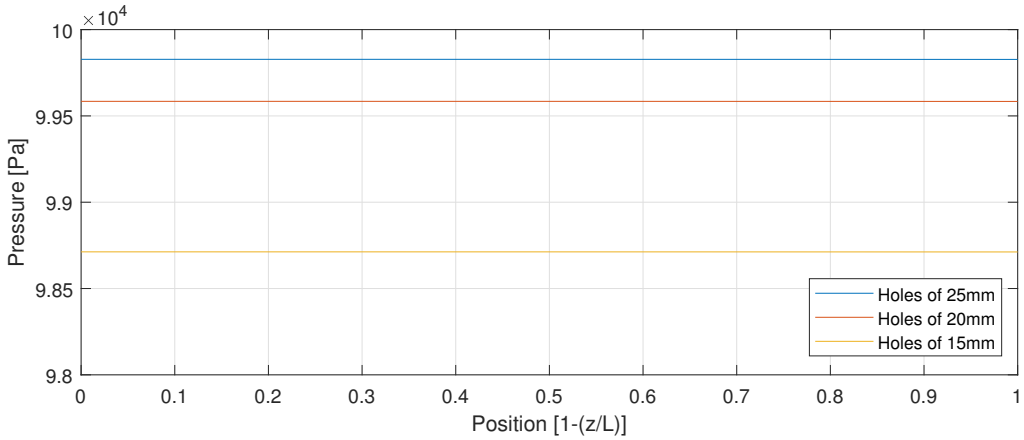

Figure 4.7: The pressure along the profile with perforations of 25mm, 20mm and 15mm

The fourth test is to vary the air density. Stated is that when the density is decreased that the pressure difference required should be lower. This is expected due to the lowered density term in both the pipe pressure loss and the hole pressure loss. In Figure 4.8 the results are shown of a density which is 5% lower compared to the density which is used for the baseline used in the second verification test. It is clear to see that the pressure is higher compared with the simulation with the standard density. This means that the required pressure difference is smaller. So this tests is passed successfully. The fifth test is a test where the kinematic viscosity is

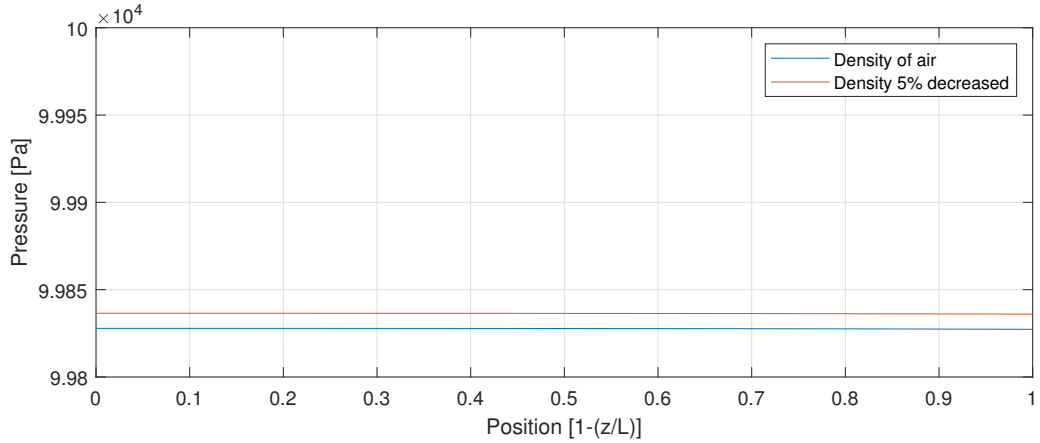

Figure 4.8: The pressure along the profile with a 5% lower density

changed. The expectation is that when the viscosity is increased the pressure will decrease. This is expected because the flow resistance will increase, so a larger pressure difference will be required. The simulation is done with a viscosity 100 times higher than used in the second verification test. Figure 4.9 shows the pressure distribution of this test. What can be seen in this pressure distribution is that at the left side the pressure is slightly higher compared to the baseline and at the right side the pressure is slightly lower. This complies with the expectation of a higher viscosity, but the effect is very small. The reason why this large variation has such a small influence on the performance can be explained by the Navier-Stokes equation. Experienced is when using this equation that at high Reynolds numbers the viscosity term can be neglected due to the insignificant influence.

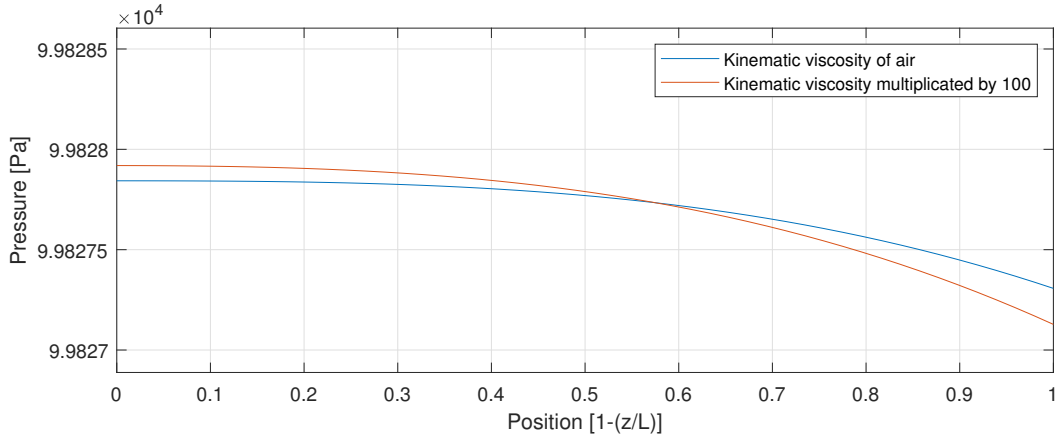

Figure 4.9: The pressure along the profile with a 100 times higher viscosity

4.3. Verification of the fan

The fan should also be verified to make sure that the behaviour is mathematically correct. This will be tested with two different tests. The first test is to simulate the static working points, and the second test will test the dynamic behaviour.

For the first test the incoming pressure is fixed and the requested C_q is varied. While varying the C_q four different outputs are monitored. These four parameters are:

1. The fan power
2. The fan efficiency
3. The volumetric flow rate
4. The rotational speed

These four outputs should help to give insight if the behaviour is as expected. Expected is that when the C_q is increased that the power, volumetric flow rate and the rotational speed will increase and also when the C_q is decreased that these outputs will decrease without an effect of hysteresis. For the efficiency is the expectation that there will be a point where it will be a optimal working point.

The C_q starts with a value of 0.047 and is increased ten times with 0.003 every 20 seconds, after this the C_q is set on 0.047 before it is lowered ten times with 0.003. In Figure 4.10 it can be seen that the power, volumetric flow rate and rotational speed increases and decreases as expected along with the C_q. Interesting is the efficiency, which has an optimum at C_q = 0.041 in this specific case. With these results it can be stated that this system has passed this verification test.

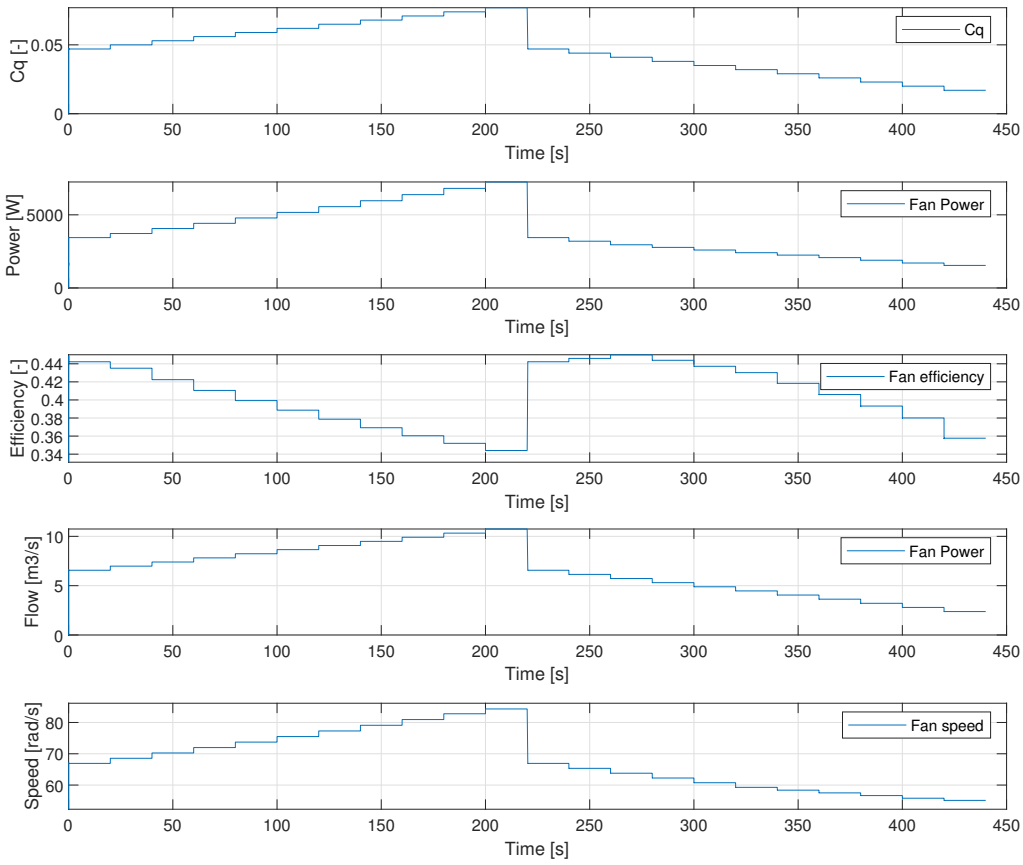

Figure 4.10: Static fan verification test

The last test is to test the dynamic behaviour of the system. This test is to check whether the inertia of the fan and motor reacts as expected when changing the pressure. Expected is that when the pressure difference is increased that the controller will increase the power to maintain the requested C_q. This effect should be visible in both the power and the rotational speed. This is modeled by changing the outside pressure at the perforation. In Figure 4.11 the simulated outside pressure is shown. Note that this is the pressure at the perforation side. The pressure at the outside of the fan is still fixed at $10 \cdot 10^4 Pa$. The rest of the input is set on the standard values.

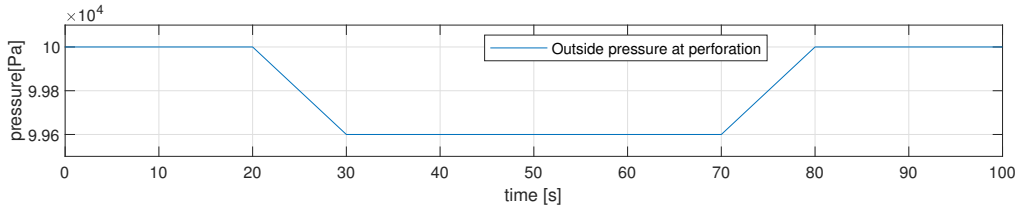

Figure 4.11: The outside pressure at the perforation used as input for the dynamic test

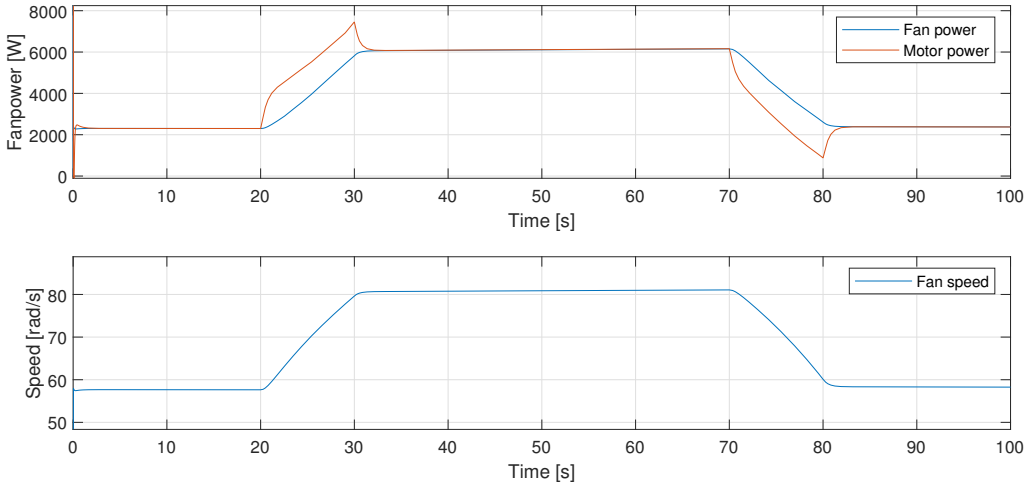

Figure 4.12: The effect of the pressure drop outside the Turbosail

The upper graph of Figure 4.12 depicts the fan and motor power and the lower graph shows the rotational speed of the fan. The system is steady for the first 20 seconds. But when the pressure at the perforation is decreased the required power is increased. This is visible in the rotational speed, which has a direct effect on the fan power. Notable is the reaction of the motor power. The motor power has a significantly different increase in power compared to the fan power. This is due to the rotational inertia of the motor and fan combined. When the rotational speed is increased the motor is not only powering the fan and some resistances, but it is also storing rotational energy into the system. When lowering the rotational speed the inertial energy is released what causes the motor to use less power. This effect is clearly visible starting from 70 seconds. The low load corresponds with an aspiration coefficient C_a of 0.36 and the higher load corresponds with a C_a of 0.97. These values are in a logical range when compared to the C_a values of Cousteau[4]. The system reacts as expected on the dynamic tests. Thus the system passed this test.

4.4. Conclusion

The performed verification has given insight in the mathematical correctness of the model. The convergence study gave insight in the sensitivity of the amount of elements, where 50 elements are chosen as sufficient for this model. After this the model has been subjected to five different tests in order to test if the model does represent the underlying mathematical model. The mass balance, logical trends in flow behaviour, and variations in density and kinematic viscosity are tested and compared with the expectation. All five test results did meet the expectation.

The verification of the fan is done in two stages. One to check the static working points and the other to check the dynamic behaviour. In the static part the fan power, fan efficiency, volume flow and rotational speed are monitored while the C_q is varied. The dynamic part investigates how the system reacts on an increase of pressure difference. Both stages resulted in simulations which complied to the expectations.

The verification process is, as mentioned earlier, an almost infinite process. This is due to the fact that it is possible to make up an enormous amount of different tests. But with every test that is passed the certainty increases that the model is mathematically correct. With this and the carefully chosen tests performed in mind it can be stated that the model is verified. In the next chapter a sensitivity analysis will be performed in order to gain insight in the effect of different parameters.

5

Sensitivity analysis

In this chapter the Simulink model is used to investigate the sensitivity of different parameters. Valuable insight can be obtained on the effects of changing different parameters of the system, although the calibration and validation have not yet been performed. The obtained information can be used for future Turbosail improvements. For instance when combined with CFD computations of the external aerodynamic performance of the Turbosail a more realistic and complete model is created. Where the main focus of that model will probably be to increase the energy efficiency of the Turbosail while maintaining or improving the performance.

Six different parameters are varied in this chapter in order to lower the energy consumption while keeping sight on the flow distribution along the length of the perforation. The power consumption is depicted by the fan power. The fan power is in steady state slightly lower compared to the motor power. This effect is due to the efficiency of the motor. These simulations will be performed at the two different wind speeds stated in Chapter 3, $5.67 m/s$ and $10.8 m/s$. After these parameter variations the results will be discussed and possible design improvements will be simulated. The following variations will be discussed:

1. Hole size
2. Number of holes
3. Pipe diameter
4. Length of the Turbosail
5. Taper
6. Thickness of the perforated plate

In Table 5.1 the used input for these parameter variations is shown. The parameters that are varied are noted as "Varied" and will be discussed in the corresponding section.

Table 5.1: The input of the parameter variation

	L [m]	D [m]	Taper [-]	Plate thickness [mm]	N - holes [-]	Hole diameter [mm]	κ [-]	Total perforated area [m^2]	w_{perf} [m]
1	10	1	0	5	2000	Varied	0.4	Varied	Varied
2	10	1	0	5	Varied	Varied	0.4	0.98	0.245
3	10	Varied	0	5	2000	25	0.4	0.98	0.245
4	Varied	1	0	5	Varied	25	0.4	Varied	0.245
5	10	Varied	Varied	5	2000	25	0.4	0.98	0.245
6	10	1	0	Varied	2000	25	0.4	0.98	0.245

5.1. Variations in hole size

Variations in geometry of the perforated plate will lead to different performances of the suction system. The first simulation compares the effect of different hole sizes with the κ and number of holes at a fixed value, which causes the width of the perforated area to increase. In Figures 5.1 and 5.2 the result of these simulations are shown. What can be seen clearly in both situations is the enormous increase in fan power necessary to overcome the decrease in hole size. This is due to the decrease in perforated area, which causes the flow speed through the holes to increase. Another major difference is the fan power compared over the two different wind speeds, the fan power is 6.5 times higher with a wind speed of $10.8 m/s$ compared to the situation at $5.67 m/s$. The left part of both figures depicts the deviation from the mean mass flow per hole. In this way the deviation in different settings can easily be compared. Noteworthy are the similarities in the mass flow distribution over the holes at both wind speeds. It can be concluded that a decrease in perforated area causes a strong increase in required power and that the flow distribution over the holes in this velocity region is not influenced by the change in wind speed when maintaining a fixed C_q.

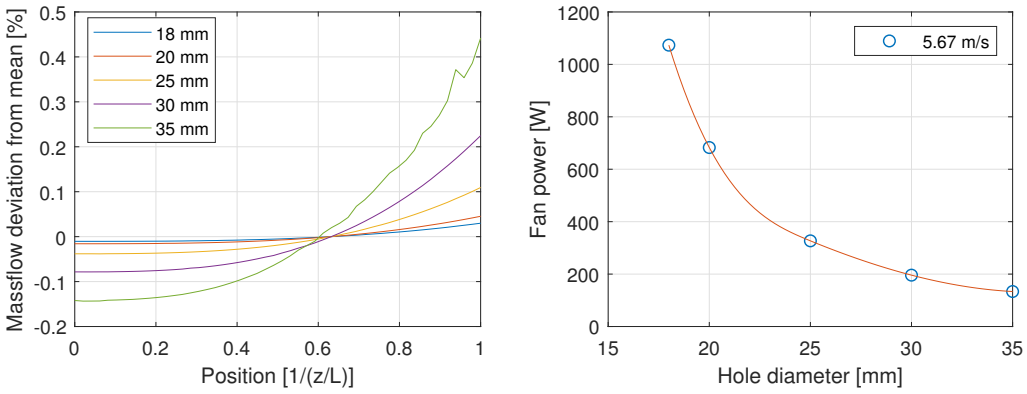

Figure 5.1: Different hole sizes at $5.67 m/s$

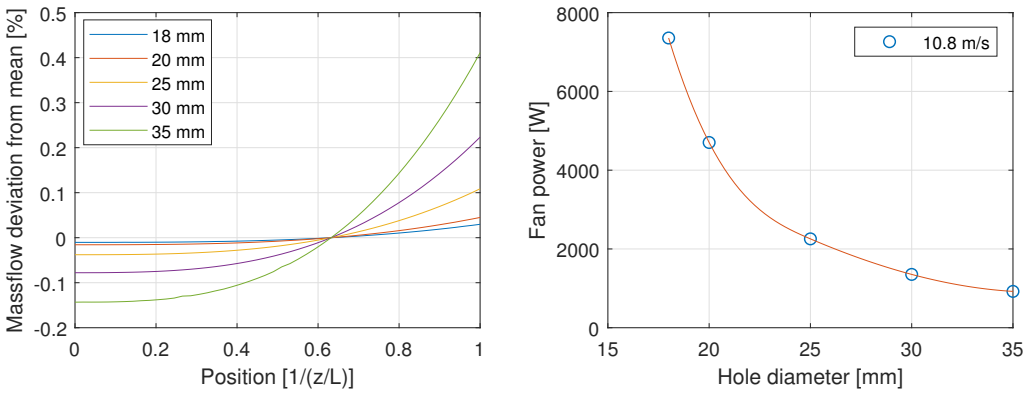

Figure 5.2: Different hole sizes at $10.8 m/s$

5.2. Changing the amount of holes

In the previous simulation it was visible that the change in hole size while maintaining an equal amount of holes has a great influence on the required power. This is due to the in- or decrease of total perforated area. When differing the amount of holes while keeping the total hole area, κ and the width of the perforation constant, insight is gained over the effect of differing the refinement of the perforation. In Figures 5.3 and 5.4 the effect of change in this parameter is shown. Simulations are performed for 500, 2000, 7000, 12000 and 20000 holes, where the largest hole diameter is 50 mm and the smallest hole diameter is 7.9 mm.

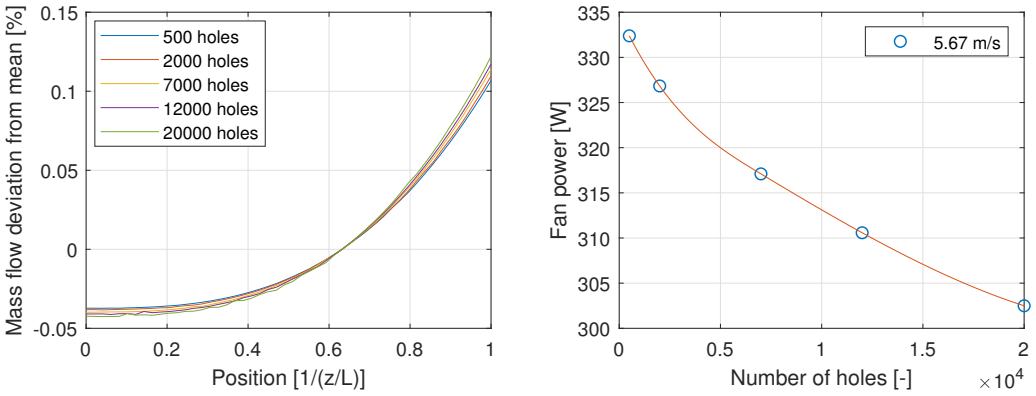

Figure 5.3: Different amount of holes at 5.67m/s

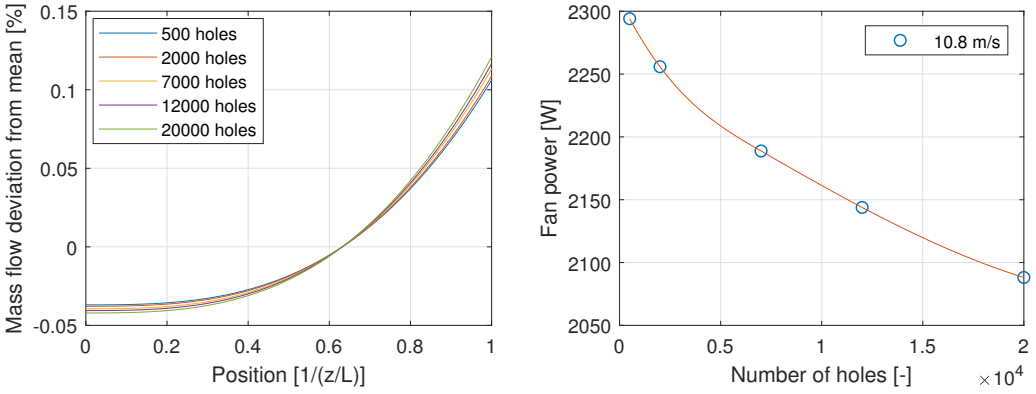

Figure 5.4: Different amount of holes at 10.8m/s

Interesting in these figures is that the simulation with the small holes require less fan power compared to the results of the simulation with large holes. This is due to the fact, which is mentioned in the verification, that the Reynolds number is very high which causes the viscosity to have an insignificant influence, what has the effect that a more refined perforated surface has a slightly lower resistance. Concluded is that a more refined perforation is preferred.

5.3. Variations in internal pipe diameter

Another case is when the inside pipe diameter is changed. In this simulation the outside geometry is fixed, but a theoretical inner tube is positioned and changed in diameter. In Figures 5.5 and 5.6 the effect of such type of system is shown. The flow distribution has a larger deviation when the internal diameter is reduced, this is due to the increase in flow speed, thus an increase in resistance. A increase in fan power of 2% is seen between 1m and 0.6m diameter. But a small decrease in diameter has a small effect on the performance. Concluded is that the pipe diameter should be as large as possible, but the disadvantageous effects are small when a decrease in diameter is necessary.

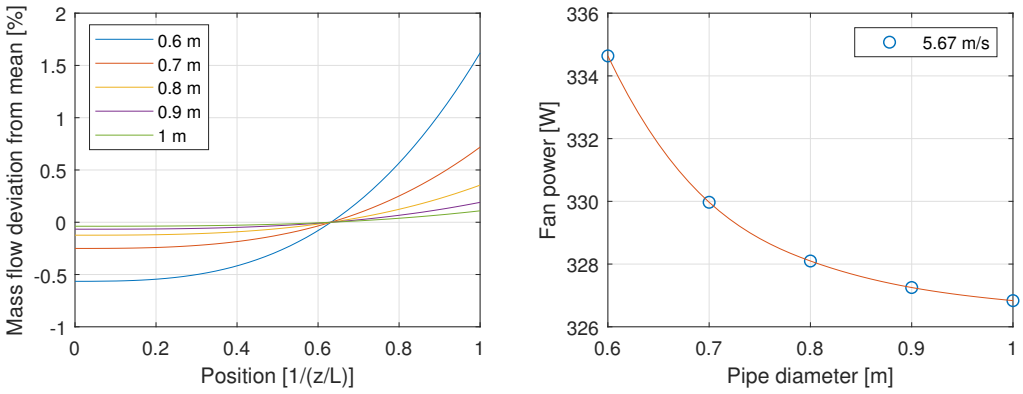

Figure 5.5: Different internal diameter sizes at 5.67m/s

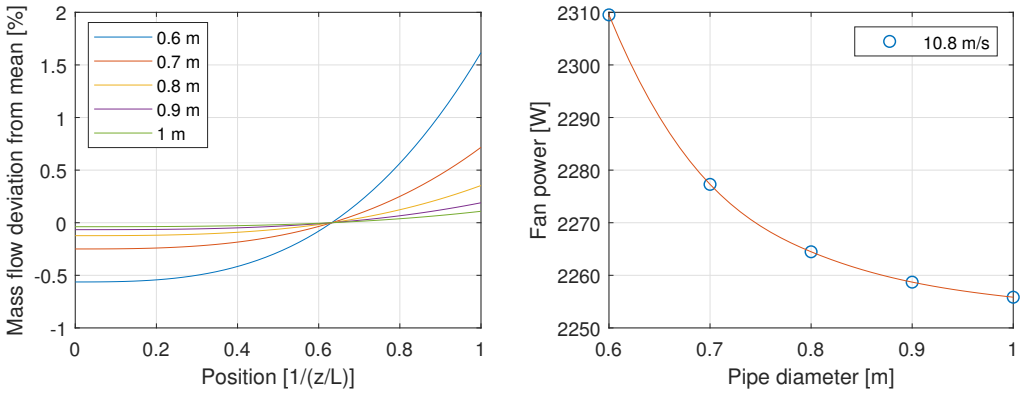

Figure 5.6: Different internal diameter sizes at 10.8m/s

5.4. Variations in length

When a new type of Turbosail is developed it is interesting to know what effect the length of the wing has on the required power. In these simulations the length of the Turbosail is differed from 5 to 25 meters. The number of holes per meter is set constant at 200 holes of 25 mm. Figures 5.7 and 5.8 depict the results of these simulations. The simulation of 5 meter length at 5.67m/s is not performed due to stability issues. When looking on the left of both Figures it can be seen that the difference in the mass flow distribution increases when the length of the Turbosail is increased, but the influence is still relatively small. More interesting however is the effect on the fan power, which is depicted as power per meter length. This is done in order to be able to compare the different situations. What can be seen at a wind speed of 10.8 m/s is a large increase in required power when the length of the Turbosail is increased to more than 10 meter. The increase in power per meter length when increasing the length in this result is that large that it is counter intuitive. The cause of this counter intuitive result will be discussed in Section 5.7.

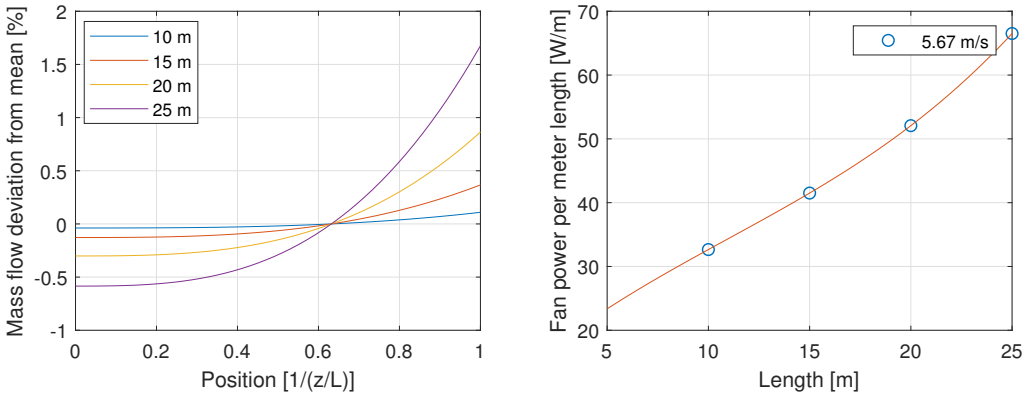

Figure 5.7: Different Turbosail lengths at 5.67m/s

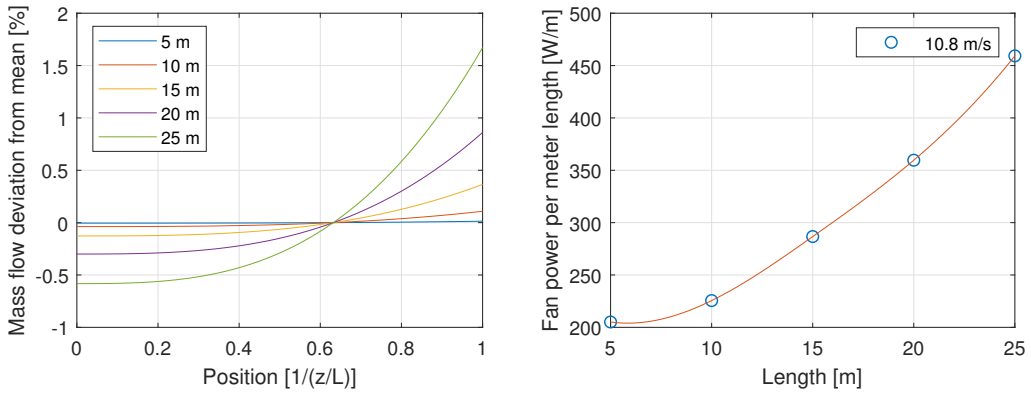

Figure 5.8: Different Turbosail lengths at 10.8m/s

5.5. Variation in Taper

Another phenomenon to look into is the effect of taper variation over the length of the Turbosail. In this simulation there are five situations discussed all with the same internal volume but with an increase in the diameter at the fan side with steps of 10%. The results of these simulations are shown in Figures 5.9 and 5.10. Interesting in the results is the effect on mass flow distribution where 0% has the largest deviation at the fan side, and 40% has the largest deviation at the top. The best flow distribution seems to be between 20% and 30%. On the right side of the Figures the effect on fan power is shown. Concluded is that the effect on power is negligible, because the power decreases with less than 0.01%.

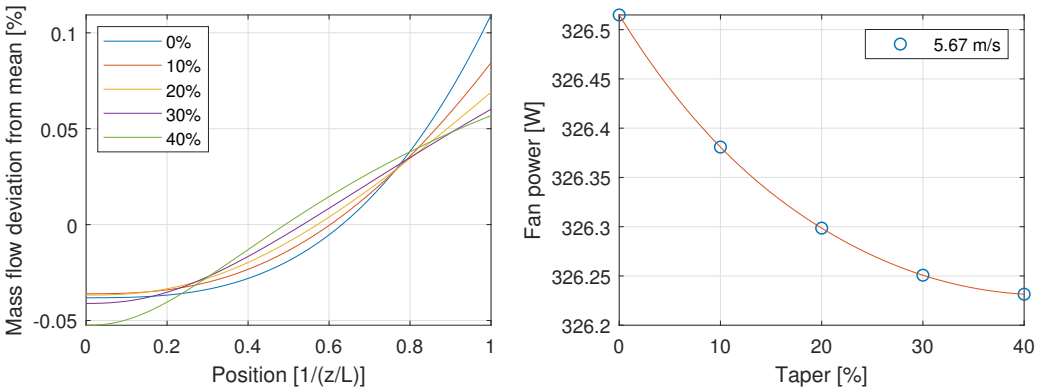

Figure 5.9: Different taper ratios at 5.67m/s

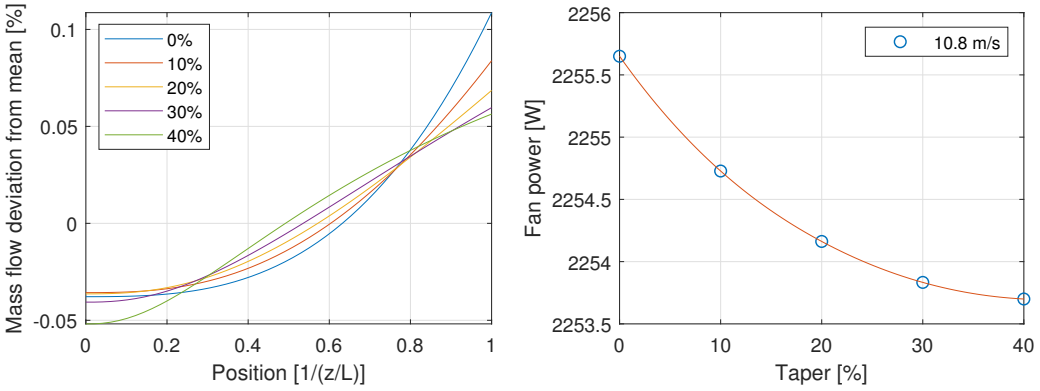

Figure 5.10: Different taper ratios at 10.8m/s

5.6. Variations in thickness of the perforated plate

The last parameter variation performed is a variation of the thickness of the perforated plate. This is done for a plate thickness from 1 to 9 millimeter and the results are shown in Figures 5.11 and 5.12. Interesting and counter intuitive is the reduction in fan power when the plate thickness is increased. This happens because of the τ term in Formula 3.18. This τ is a value which comes from a look up table in the Handbook of Hydraulic Resistance[11] and decreases when the length over diameter term increases. What results in a lower ζ thus a decrease in pressure drop. The disadvantage of an increase in plate thickness is the gain of weight of the system. As mentioned earlier, the formula used form the Handbook of Hydraulic resistance is old and possibly incorrect. With that in mind, no conclusion is made and more research will be required on this topic.

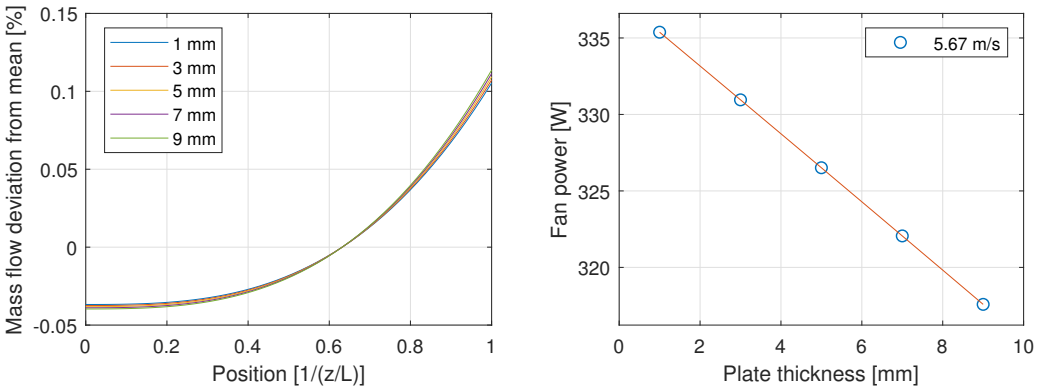

Figure 5.11: Different plate thicknesses at 5.67m/s

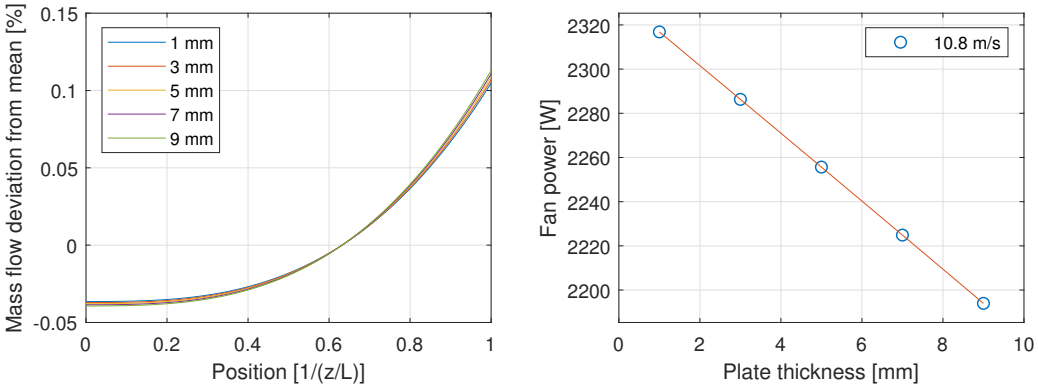

Figure 5.12: Different plate thicknesses at 10.8m/s

5.7. The effect of fan efficiency

A single fan efficiency characteristic is used in the simulations of the parameter variations above. The efficiency of this fan is calculated by using the dimensionless pressure π_2 (Eq. 3.19). The used fan characteristic has an optimal efficiency at a certain point. But some of the simulations took place outside of the efficient region of this fan. Where another type of fan may perform at a higher efficiency in these situations. To eliminate false results due to this effect all simulations are repeated but in this case with the efficiency fixed at 45%. In Figure 5.13 the six results at 10.8 m/s are shown. It is clear that there is almost no change in the consumption trend when varying the hole diameter, the amount of holes, the tube diameter, the plate thickness or the taper. But the difference in result on the effect of varying the length is large, this is due to the inefficiency of the chosen fan at higher pressure differences. With these "new" results it can be seen that the length of the wing does not have an enormous effect. But still an increase of power per meter length is seen when the length is increased. Thus it is concluded that a increase length of the Turbosail does have a negative effect on the power consumption per meter length.

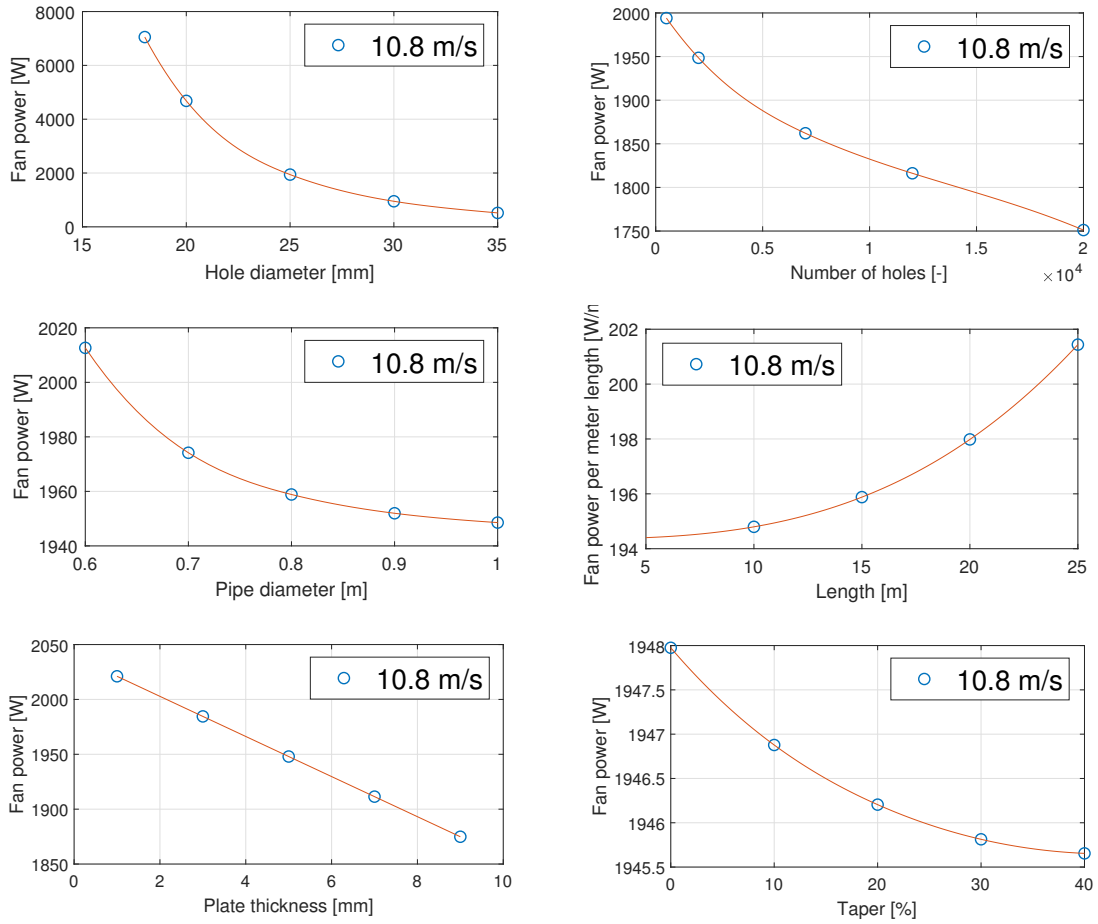

Figure 5.13: The parameter variation results at 10.8 m/s with fixed efficiency

5.8. Improved design

With the knowledge gained in the previous parameter variations it is possible to propose one or more different designs in order to increase the energy efficiency. First the effects of each parameter will be discussed, after this a simulation is performed with these new found parameters in order to visualize the effect that different parameters have on flow distribution and energy consumption.

From the variation in hole size it is concluded that a large total perforated area will give a low power consumption at cost of a slight increase in difference of the mass flow distribution over the length. Combined with the knowledge that a large number of small holes has a better performance compared to the same perforated area with a larger hole diameter, it can be stated that a large number of small holes with a high total perforated area is considered the preferred situation. The pipe diameter gives the small but expected result to make it as large as possible. The larger contributing parameter to increase energy efficiency of the suction system is the length of the suction system. Here is found that increasing the length of the sail does increase the required power per meter length. At last the thickness of the perforated plate was considered, where a trend of increasing the plate thickness caused a small decrease in required power.

To make an improved design it is necessary to compare the system with a baseline, in this case the Turbosail of Econowind called the 'Ventifoil' of which two are fit into a 40 foot container. This gives a limitation in size, because the sail itself cannot be longer than 11 meter, the diameter must be kept around 1 meter in order to fit two sails next to each other. The suction of this system is performed by a single fan at the bottom. Due to the lack of information the parameters of this Turbosail are estimated at 2000 holes with a diameter of 24 mm, a length of 11 meter, a wall thickness of 3 mm and a taper of 20%.

From this baseline the parameters have to be tuned in order to minimize the power consumption at equal or improved performance. The first improved design has equal outer dimensions compared to the base line, but the amount of holes is increased such that holes of 5 mm are used, and when keeping the perforated surface equal to the baseline this gives an amount of 46080 holes. The perforated surface is kept equal in these simulations in order to visualize the effect of the other parameters. An increase in perforated surface will definitely lower the energy consumption.

Another more challenging design is a design with two fans, this is chosen because the increase of fan power per meter length of Turbosail. The rest of the parameters are kept equal to the first improved version, but in this case there is not only a fan at the bottom of the Turbosail, but also one at the top. To be able to model this, the model is divided into two separate wings which are combined in the result. Because of practical reasons there is a theoretical plate in the middle of the Turbosail which disables a flow between the two halves.

In Figure 5.14 the mass flow distributions of the three discussed situations is depicted. When comparing Design 1, the baseline, with Design 2 it can be seen that the improved design results in a small increase of flow variation over the length. But the power consumption of the first design is 449 Watt and the consumption of the second design is 400 Watt, both at 5.67 m/s, which means a reduction of 10.9%. And the power consumption at 10.8 m/s are respectively 3104 Watt and 2764 Watt, what yields a reduction in required power of 11.0%. The third design has an interesting flow distribution due to the two separate systems. Right side of the figure, that depicts the lower half of the Turbosail, has a relatively small deviation. But the left side, that depicts the upper half of the Turbosail, has a larger difference in mass flow distribution. This is due to the taper of the Turbosail, which causes a decrease in pipe diameter closer at the fan where the flow is increasing. The energy consumption of this design is at 5.67 m/s as low as 399.5 Watt and at 10.8 m/s it is 2761 Watt, which are both reductions of 11.0% compared to the baseline.

All of these simulations are performed with a fan working at a fixed efficiency of 45% to be able to compare the different situations with each other. This result means that for a Turbosail with these geometric properties both the second and third design will be interesting if a fan is used which is efficient in the right domain.

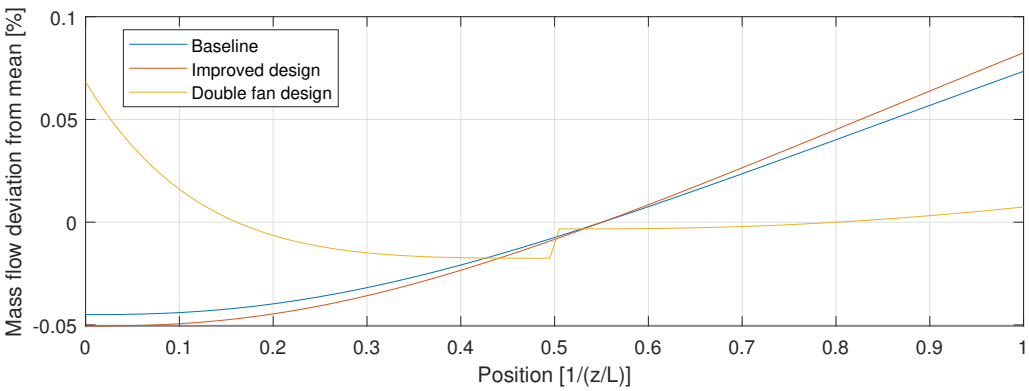

Figure 5.14: The mass flow distribution in three different designs

6

Conclusion and Recommendations

The flow behaviour and performance of the suction system of a Turbosail has been investigated using Matlab Simulink simulations. This chapter describes the conclusions made after this investigation and provides recommendations for future Turbosail research.

6.1. Conclusions

In order to improve the performance of the current Turbosail design a literature study has been performed. Found is that a lot of research has been performed on flow behaviour on the outside of the Turbosail where major assumptions have been made on the suction system. In most cases the suction system was simplified to a slot or perforation with a uniform incoming flow. To increase the performance of current Turbosail design more knowledge is required of the suction system.

The aim of this research, as stated in Chapter 2, is to gain insight in the behaviour of the internal suction system and its effect on the total system performance. Where the first research question is:
"How can the relation between the outside geometry, the inside geometry, the fan and the drive be described and modelled?"
To answer this question, a lumped parameter approach is chosen and is used in Chapter 3 to yield a model in Matlab Simulink. This model is verified in Chapter 4 using a range of verification tests. The first part of this verification was to check whether the model converges and to determine what amount of elements is required. In Figures 4.3, 4.4 and 4.5 the results of these simulations are shown and is concluded that 50 elements is sufficient for this research.
The second part of the verification has tested the mathematical correctness of the model. This is done with 5 different tests. These tests can be found in Section 4.2 and are passed with success. In Section 4.3 the fan is verified in a static and dynamic situation. The static verification verifies different static working point set by changing the suction coefficient C_q to set values while monitoring the power consumption, efficiency, volumetric flow and rotational speed. The dynamic verification tested the effect of inertia of the fan system. All verification phases have been passed with thus it can be concluded that the model is sufficiently verified. The consecutive step after the verification is the model calibration and validation. Due to a lack of resources and time these phases have not been performed yet. But, a description of these proposed phases can be found in Appendix A. With these steps performed the first research question can be answered: The relation between the outside geometry, the inside geometry, the fan and the drive can be described and modelled using a lumped parameter method and implementing this in Matlab Simulink.

The second research question is:
"How sensitive is the total suction system for variations of different parameters?"
To answer this question, a sensitivity analysis is performed to gain insight in the sensitivity of six different parameters of the system.

The first analysis was a variation in hole size while maintaining a fixed number of holes. This resulted, as can be seen in Figures 5.1 and 5.2, in a strong increase in required power when decreasing the hole diameter.

It is concluded that larger holes are favourable when power consumption is important. But when the hole size is chosen too large, large deviations in mass flow may occur. The second analysis was to investigate the effect of differing the number of holes in the perforation while maintaining the same perforated area, κ and width of the perforated plate. Concluded is that a large number of small holes is favorable over a small number of large holes. As is shown in Figures 5.3 and 5.4 the fan power changes up to 10%. The third analysis was about varying the internal pipe diameter. This resulted, as shown in Figures 5.5 and 5.6 in an increase up to 2% in required power when the internal diameter is decreased. Concluded is that the increase in fan power is negligible when a small decrease in internal pipe diameter is applied. The fourth analysis was a variation in length of the Turbosail. In Section 5.4 a large increase in required power was found when the length of the Turbosail was increased. This result was unrepresentative due to the effect of the fan efficiency. In Figure 5.13 the result with a fixed fan efficiency is shown, clear is that the increase of fan power is significantly lower compared to the result of Section 5.4. But, the final conclusion is that an increase in required power of more than 2% is shown when the length of the Turbosail is increased. The fifth analysis was to investigate the effect of a variation in taper. The taper turns out to have a negligible effect on the required power, but an increase in taper has a positive effect on the mass flow distribution along the length of the Turbosail as is seen in Figures 5.9 and 5.10. The last analysis is a variation in thickness of the perforated plate. The influence of an increase in plate thickness gives in this model a decrease in required power of up to 5%. As experienced, the effect of fan efficiency at different pressures proved it self to be of great importance. A mismatch of this efficiency region easily causes the required power for this model to multiply by 2.5.

Two different setups are designed using the knowledge of the parameter variations and these are compared to the container unit of Econowind. Energy savings of 11% are achieved using the same perforated area compared the the Econowind unit. Larger energy savings can be realized when the perforated area is increased.

6.2. Recommendations

The recommendations can be divided into two parts, one with recommendations for the improvement of the model, the other with recommendations for the future Turbosail designs.

6.2.1. Model improvement

The model created is a solid and successfully verified model. However there are recommendations for model improvement and further investigation.

- The model should be calibrated and validated. These phases are described in the appendix and will contribute to the quality and reliability of the model.
- Research should be done to determine an improved method to calculate the flow resistance through a perforated plate.
- The resistance of the flow through the perforated plate may be influenced by the tangential flow over the perforation. In the current model an assumption is made to account for these effects. But this could be improved when more knowledge is gained on the effect of such a cross-wind.
- The effect of extreme designs like a slot instead of holes will be interesting to simulate.
- At low flow velocity difficulties can be encountered in terms of numerical stability. It will be an improvement when these issues are fixed.
- When the model could be converted to interact with the current CFD calculations valuable insight will be obtained on the total system behaviour.

6.2.2. Future Turbosail designs

A number of recommendations on the design for a future Turbosail unit can be given with the knowledge of this thesis. The following items represent the key considerations and possible improvements.

- The matching of the fan is of great importance: A fan with a wide efficiency region is preferred.
- Multiple fans could be interesting, but this may increase the weight of the system.
- The perforated area should be maximized because this gives a large decrease in required power.

A

Proposed calibration and validation

As stated in the previous chapter :The verification, calibration and validation process are of great importance to assess the correctness and usefulness of a model. This chapter discusses, ongoing on the successful verification performed in Chapter 4, the proposed calibration and validation process. The calibration and validation will not be executed due to the lack of time and resources. The first section discusses the calibration process and the second section will discusses the validation process.

A.1. Calibration

The calibration phase is necessary to improve the results of the model to correspond with reality. Or as stated by Ben H. Thacker et al.: "Calibration: Process of adjusting numerical or physical modelling parameters in the computational model for the purpose of improving agreement with experimental data" [24]. To perform this step two fundamental ingredients are required. The first important ingredient is the model that has to be calibrated. This will not be a problem because the model is made in Chapter 3 and verified in Chapter 4. But there is, as stated by Ben H. Thacker et al., also experimental data required. This data is not available, so this section will describe the proposed calibration process.

The first step is to enter the geometrical data of the experiment into the Simulink model. Length, diameter (hydraulic diameter) of the Turbosail, taper, number of holes, hole diameter, thickness of the wall, κ, the surface roughness and the fan diameter. Recommended is to perform the calibration at a wind speed of $10.8 m/s$ and with a suction coefficient C_q of 0.047. The temperature of the air inside the experiment should also be entered into the Simulink model.

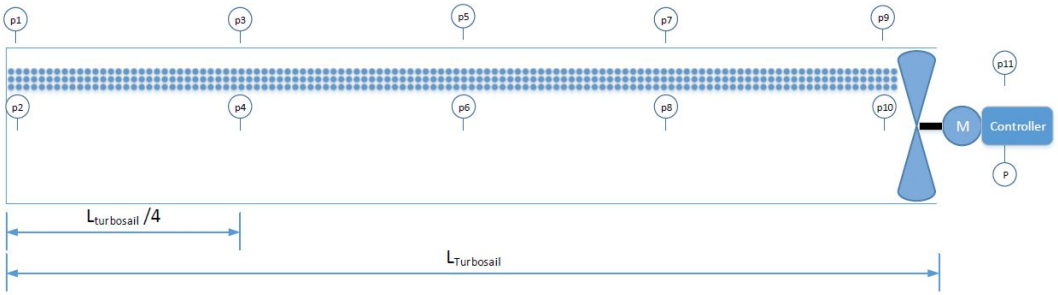

Figure A.1: The placement of sensors along the Turbosail

Carefully chosen data is required to perform a valuable calibration in order to fine tune the different parts of the model. The aim is to get data for each individual subsystem, this to decrease the chance of getting the correct results with a false input. To obtain this information 11 pressure sensors and an electrical power sensor are recommended. The placement of these sensors is displayed in Figure A.1. Five sets of pressure sensors are placed along the Turbosail. One sensor inside the wing and another one outside the wing. At the fan there is one pressure sensor and one sensor to measure the electrical power.

The five sets of pressure sensors are used to obtain different parts of information. The five sensors outside of the Turbosail are used to implement the outside pressure distribution. This information is used as input for the Simulink model. The pressure drop through the perforations is obtained when comparing the inside and outside pressure of a sensor set. And when comparing the five sensors inside the Turbosail the pressure gradient along the length of Turbosail is obtained. This can be compared with the results of the simulation and that information can be used to make the Simulink model to correspond with the experiment.

The calibration of the fan starts with entering the information of installed fan of the experiment. The π_2 to π_1 table and the π_2 to η_{Fan} table have to be calculated and programmed. After this the information of the experiment can be used to fine tune the system. With a known motor efficiency it is possible to calculate possible extra losses in the system using the pressure difference between p10 and p11 and the consumed electrical power.

With all this information it is possible to calibrate the Simulink model in order to match the result with the result of the experiment. Parameters like the "Zeta correction factor" can be used to make the pressure drop through the perforation fit. Therefor extra correction factors have to be introduced in order to make the calibration complete.

A.2. Validation

With the calibration performed the Simulink model should be Validated. "Validation: The process of determining the degree to which a model is an accurate representation of the real world from the perspective of the intended uses of the model."[18]. This statement is written by William L Oberkampf et al. and gives a good description of what validation is. A simulation model is practically always made with simplifications and assumptions. This has the effect that such a model will never represent reality perfectly. Despite this a model can still be used, but it is necessary for the users to know how accurate the computations are.

For this validation phase the same wind tunnel setup as in the calibration process can be used. This phase can be divided in two phases. The first phase is to compare different static working points. This is done to check whether the Simulink model models correctly at different working points than the ones used in the calibration phase. The second phase is a test where the dynamic behaviour is tested. This is to determine whether the dynamic behaviour of the experimental setup matches the behaviour of the Simulink model.

The first validation tests are designed to compare the static working points of the experimental setup and the Simulink model. The experiment setup is the same as used for the calibration. But this time different wind speeds are used. The calibration is performed at $10.8 m/s$. Recommended is to perform tests at a low speed $3 m/s$, at the most occurring speed $5.67 m/s$ and at a high wind speed of $15 m/s$. All with a C_q of 0.047.

With these three working points experimental data can be obtained and simulated data can be computed which is used to determine the deviation between experimental and computational data. This assessment gives insight if and in what extend the model computations meets the experimental data.

The next part of the validation is to investigate whether and to what extend the dynamic behaviour of the model equals with the results of the experiment. Here it is important to make sure that the controllers in both systems have the same characteristics in order to be able to compare both dynamics behaviours with each other. Now tests can be performed with a varying wind speed over time simulating wind gusts in the experimental setup. This will have an effect on both the pressure outside the perforation and on the required volume flow in order to maintain the given C_q of 0.047. The pressure profile that is experienced in the experiment should be used as input in the Simulink model. This will result in a simulation of the same circumstances. Now the used power and the pressure on both sides of the fan (p10 and p11) will give insight in whether extend the simulation data equals the experimental data in terms of fan behaviour.

With these two validation phases performed enough information should be obtained to give the user insight of the usefulness of the model. And with this in mind choice can be made if the model will be used, or if the model requires a revision.

Bibliography

[1] Adk ventilatoren - catalogus. https://almeco.eu/nl/system/files/files/downloads/adk_en_1.pdf. Accessed: 2019-6-24.

[2] Boundary layer separation on aircraft wings. https://www.razvanapetrei.com/boundary-layer-separation-over-aircraft-wings/. Accessed: 2019-9-24.

[3] Alyson Azzara, Dan Rutherford, and Haifeng Wang. Feasibility of imo annex vi tier iii implementation using selective catalytic reduction. *The International Council on Clean Transportation, Washington, DC, Working Paper*, 4, 2014.

[4] Bertrand Charrier, Jacques Constans, Jacques-Yves Cousteau, Abdallah Daïf, Lucien Malavard, and Jean-Luc Quinio. Fondation cousteau and windship propulsion 1980–1985 system cousteau-pechiney. *Journal of wind engineering and industrial aerodynamics*, 20(1-3):39–60, 1985.

[5] Econowind. Maritime innovation award 2019, 2019. URL https://www.econowind.nl/index.php/2019/11/05/award-winner/. [Online; accessed January 26, 2020].

[6] Ouahiba Guerri, Erwan Liberge, and Aziz Hamdouni. Numerical simulation of the turbulent flow around an oval-sail. *Journal of Applied Fluid Mechanics*, 9(4), 2016.

[7] Cherif Hcini, Essia Abidi, Badreddine Kamoun, and David Afungchui. Numerical prediction for the aerodynamic performance of turbosail type wind turbine using a vortex model. *Energy*, 109:287–293, 2016.

[8] Cherif Hcini, Essia Abidi, Badreddine Kamoun, and David Afungchui. A turbosail profile analysis code based on the panel method. *Energy*, 118:147–155, 2017.

[9] Jerzy Herdzik. Emissions from marine engines versus imo certification and requirements of tier 3. *Journal of KONES*, 18:161–167, 2011.

[10] Russell C Hibbeler. *Fluid Mechanics in SI Units*. Pearson Education India, 2017.

[11] IE Idelcik. Handbook of hydraulic resistance: coefficients of local resistance and of friction. Technical report, ERDA Div. Phys. Res., 1966.

[12] Anton Kisjes. Wind propulsion for merchant vessels: Assesing the performance of a ventifoil for wind assisted propulsion. Master's thesis, TU Delft, the Netherlands, 2017.

[13] Laurens-Jan Lagendijk. Performance investigation of ventifoil ship propulsion: Research into the propulsive performance of ventifoils using cfd simulations. Master's thesis, TU Delft, the Netherlands, 2018.

[14] EN Lightfoot, PS Thorne, and LL Stoll. Dimensionless presentation of performance data for fans and blowers. *AIChE journal*, 30(2):341–345, 1984.

[15] HT Low, SC Luo, and SH Winoto. Flow past a wind-assisted ship propulsion device. *Ocean engineering*, 18(6):555–565, 1991.

[16] L Malavard. Un nouveau propulseur éolien de navire, la vie des sciences. *CR Ser. Générale*, 1:57–72, 1984.

[17] Bengamin I Moat, Margaret J Yelland, and Anthony F Molland. Quantifying the airflow distortion over merchant ships. part ii: Application of the model results. *Journal of Atmospheric and Oceanic Technology*, 23(3):351–360, 2006.

[18] William L Oberkampf, Timothy G Trucano, and Charles Hirsch. Verification, validation, and predictive capability in computational engineering and physics. *Applied Mechanics Reviews*, 57(5):345–384, 2004.

[19] Reuters. German ship fights climate change with high-tech kite, 2007. URL https://www.reuters.com/article/us-climate-germany-ship/german-ship-fights-climate-change-with-high-tech-kite-idUSL1548100520071217?sp=true. [Online; accessed December 2, 2019].

[20] Sailing-cargo. Redefining the understanding of maritime shipping, 2007. URL http://www.sailing-cargo.de/innovation/. [Online; accessed December 2, 2019].

[21] Stewart Schlesinger. Terminology for model credibility. *Simulation*, 32(3):103–104, 1979.

[22] Tsukasa Shiii, Hikaru Yagi, and Akihiko Fujii. Wind tunnel study of column–type circular cylinder propulsion assistance system (cpas) for ships. In *The fourth International Symposium on Computational wind Engineering Yokahama*, 2006.

[23] Douwe Stapersma. Flow systems, modelling & simulation in marine engineering. 2015.

[24] Ben H Thacker, Scott W Doebling, Francois M Hemez, Mark C Anderson, Jason E Pepin, and Edward A Rodriguez. Concepts of model verification and validation. Technical report, Los Alamos National Lab., 2004.

[25] Det Norske Veritas. Environmental conditions and environmental loads, dnv-rp-c205. *Recommended Practice, October*, 2010.

[26] Worldmaritimeaffairs. Flettner rotor for ship : The magnus effect, 2019. URL https://www.worldmaritimeaffairs.com/flettner-rotor-for-ship-the-magnus-effect/. [Online; accessed December 2, 2019].